Synthesis, Structural Diversity, Dynamics, and Acidity of the M(II) and M(IV) Complexes [MH$_3$(PR$_3$)$_4$]$^+$ (M = Fe, Ru, Os; R = Me, Et)

Dmitry G. Gusev,[†] **Rainer Hübener, Peter Burger, Olli Orama,**[‡] **and Heinz Berke***

Contribution from the Anorganisch-Chemisches Institut, Universität Zürich, Winterthurerstrasse 190, CH-8057 Zurich, Switzerland

Received October 23, 1996[⊗]

Abstract: The syntheses of complexes MH$_2$L$_4$ and their protonated analogues [MH$_3$L$_4$]$^+$ (M = Fe (**1**), Ru (**2**), Os (**3**); R = Me (**a**), Et (**b**)) are described. The structures of **1a**, **1b**, and **3a** were determined in X-ray diffraction studies. The solution structures of complexes **1**−**3** were established by detailed NMR investigations. **1a**, **2b**, and **3a** form equilibrium mixtures of two isomers in solution. The iron (**1a**) and ruthenium (**2b**) complexes isomerize between six-coordinate M(II) dihydrogen *cis*-[MH(H$_2$)L$_4$]$^+$ and seven-coordinate M(IV) trihydride [M(H)$_3$L$_4$]$^+$ molecular geometries: the first is a distorted octahedron and the second can be viewed as a hydride-capped M(PR$_3$)$_4$ tetrahedron. Complex **3a** is a pentagonal bipyramidal trihydride *cis*-[Os(H)$_3$(PMe$_3$)$_4$]$^+$ in equilibrium with the hydride-capped tetrahedral structural form. Trihydrides **1b** and **3b** are exclusively represented by the latter structural type. The cationic molecule **2a** corresponds to a dihydrogen complex *cis*-[RuH(H$_2$)(PMe$_3$)$_4$]$^+$. The metal fragment [MH-(PR$_3$)$_4$]$^+$ is thus most reactive toward oxidative addition of H$_2$ for osmium and iron, with a notably lower ability to reduce H$_2$ for ruthenium. This trend and related properties are due to electronic rather than steric factors. All [MH$_3$(PR$_3$)$_4$]$^+$ species (**1**−**3**) are fluxional in solution. The intramolecular hydride exchanges and isomerizations were studied between 20 and −140 °C and quantitatively described in terms of their activation parameters. On the basis of these, mechanistic interpretations are provided. Finally the acid/base properties of the [MH$_3$(PR$_3$)$_4$]$^+$/M(H)$_2$-(PR$_3$)$_4$ systems were established in a series of NMR experiments in THF-d_8. The pK_a values range from 10.3 to 12.9 units and increase in the following order: **1a** (10.3) < **2b** (10.7) < **2a** (10.9) < **3a** (11.2) < **3b** (12.9). This series demonstrates a higher acidity than that of the related [MH(H$_2$)(PP)$_2$]$^+$ molecules with bidentate ligands. The complexes with monodentate phosphine ligands [MH$_3$(PR$_3$)$_4$]$^+$ (**1**−**3**) represent a new and distinguished family with structural, dynamic, and acid/base properties remarkably different from most of the other known [MH$_3$L$_4$]$^+$ representatives.

I. Introduction

In the last 30 years, a number of fundamental developments in the chemistry of metal hydrides have been associated with iron, ruthenium, and osmium complexes of the general formula [MH$_2$L$_4$] and [MH$_3$L$_4$]$^+$ (L$_4$ = mono- to tetradentate phosphorus ligands). Among the most significant are the pioneering dynamic NMR studies of stereochemically nonrigid dihydrides [MH$_2$L$_4$],[1] some of the very first reliably structurally characterized examples of coordinated H$_2$,[2] and related to the former studies on the acidity of the "nonclassical" hydrides.[3] This list would be incomplete without mentioning of the rich synthetic chemistry supported by the structural and spectroscopic methodologies.[1−3] The Fe−Ru−Os triad has always attracted attention for systematic investigations which intended to evaluate

periodic trends. Thus, more recently, the structure of [MH$_3$L$_4$]$^+$ has additionally become subject of theoretical studies where the relative stabilities of the six- and seven-coordinate isomers (Scheme 1) have been determined on the basis of *ab initio* calculations.[4]

From the theoretical results it can be concluded[4a,c] that the two molecules, [FeH$_3$(PH$_3$)$_4$]$^+$ and [RuH$_3$(PH$_3$)$_4$]$^+$, should prefer different structures: the *cis*-H,H$_2$ structural type C_n, (cis,

(1) (a) Tebbe, F. N.; Meakin, P.; Jesson, J. P.; Muetterties, E. L. *J. Am. Chem. Soc.* **1970**, *92*, 1068. (b) Meakin, P.; Guggenberger, L. J.; Jesson, J. P.; Gerlach, D. H.; Tebbe, F. N.; Peet, W. G.; Muetterties, E. L. *J. Am. Chem. Soc.* **1970**, *92*, 3482. (c) Meakin, P.; Muetterties, E. L.; Tebbe, F. N.; Jesson, J. P. *J. Am. Chem. Soc.* **1971**, *93*, 4701. (d) Meakin, P.; Muetterties, E. L.; Jesson, J. P. *J. Am. Chem. Soc.* **1973**, *95*, 75.
(2) (a) Morris, R. H.; Sawyer, J. F.; Shiralian, M.; Zubkowski, J. D. *J. Am. Chem. Soc.* **1985**, *107*, 5581. (b) Ricci, J. S.; Koetzle, T. F.; Bautista, M. T.; Hofstede, T. M.; Morris, R. H.; Sawyer, J. F. *J. Am. Chem. Soc.* **1989**, *111*, 8823. (c) Bautista, M. T.; Earl, K. A.; Maltby, P. A.; Morris, R. H.; Schweitzer, C. T.; Sella, A. *J. Am. Chem. Soc.* **1988**, *110*, 7031.

(3) (a) Baker, M. V.; Field, L. D.; Young, D. J. *J. Chem. Soc., Chem. Commun.* **1988**, 546. (b) Morris, R. H. *Inorg. Chem.* **1992**, *31*, 1471. (c) Cappellani, E. P.; Drouin, S. D.; Jia, G.; Maltby, P. A.; Morris, R. H.; Schweitzer, C. T. *J. Am. Chem. Soc.* **1994**, *116*, 3375. (d) Field, L. D.; Hambley, T. W.; Yau, B. C. K. *Inorg. Chem.* **1994**, *33*, 2009.
(4) (a) Maseras, F.; Duran, M.; Lledós, A.; Bertrán, J. *J. Am. Chem. Soc.* **1991**, *113*, 2879. (b) Maseras, F.; Duran, M.; Lledós, A.; Bertrán, J. *J. Am. Chem. Soc.* **1992**, *114*, 2922. (c) Maseras, F.; Koga, N.; Morokuma, K. *Organometallics* **1994**, *13*, 4008.
(5) Albertin, G.; Antoniutti, S.; Bordignon, E. *J. Am. Chem. Soc.* **1989**, *111*, 2072.
(6) Osakada, K.; Ohshiro, K.; Yamamoto, A. *Organometallics* **1991**, *10*, 404.
(7) (a) Amendola, P.; Antoniutti, S.; Albertin, G.; Bordignon, E. *Inorg. Chem.* **1990**, *29*, 318. (b) Albertin, G.; Antoniutti, S.; Baldan, D.; Bordignon, E. *Inorg. Chem.* **1995**, *34*, 6205.
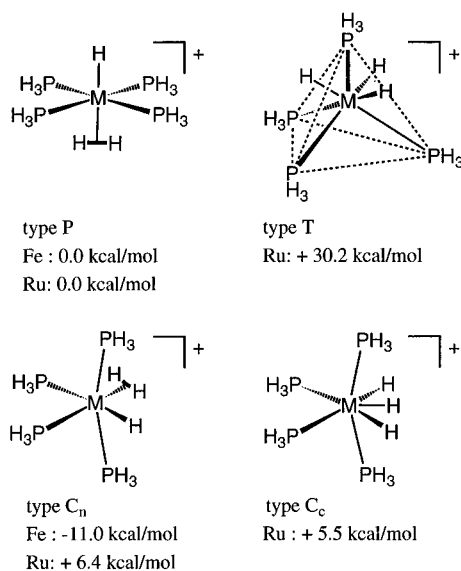(8) (a) Werner, H.; Gotzig, J. *Organometallics* **1983**, *2*, 547. (b) Desrosiers, P. J.; Shinomoto, R. S.; Deming, M. A.; Flood, T. C. *Organometallics* **1989**, *8*, 2861.
(9) Siedle, A. R.; Newmark, R. A.; Pignolet, L. H. *Inorg. Chem.* **1986**, *25*, 3412.
(10) Hills, A.; Hughes, D. L.; Jimenez-Tenorio, M.; Leigh, G. J.; Rowley, A. T. *J. Chem. Soc., Dalton Trans.* **1993**, 3041.
(11) Bautista, M. T.; Cappellani, E. P.; Drouin, S. D.; Morris, R. H.; Schweitzer, C. T.; Sella, A.; Zubkowski, J. *J. Am. Chem. Soc.* **1991**, *113*, 4876.

Scheme 1

type P
Fe : 0.0 kcal/mol
Ru: 0.0 kcal/mol

type T
Ru: + 30.2 kcal/mol

type C_n
Fe : -11.0 kcal/mol
Ru: + 6.4 kcal/mol

type C_c
Ru : + 5.5 kcal/mol

nonclassical type) and the *trans*-H,H₂ structural type *P*, respectively (see computed relative energies in Scheme 1). The symbol *P* indicates a planar or pseudoplanar arrangement of four PH₃. The classical seven-coordinate alternatives (structural types with a tetrahedral PH₃ arrangment, *T*, and classical *cis*-trihydride, C_c) were found at appreciably higher energies. These results do not easily match experimental findings.

Most of the known [MH₃L₄]⁺ (collected in Table 1) are *preferentially* of the *P* geometry. With some exceptions,[17g] tetradentate phosphorus ligands normally induce C_n structures. A number of molecules (with dcpe, diop, dppf, and PPh₃ ligands, see Table 1) demonstrate a tendency to adopt the *T* structure for increasing bulkiness of the phosphines. This is, to a certain extent, driven by the steric forces.

Most unfortunate for the examination of the theoretical results is the absence of detailed structural data for [MH₃P₄]⁺ with small monodentate PR₃ ligands, for which the PH₃ system normally provides the stereoelectronic model. For instance, [FeH₃(PMe₃)₄]⁺ was previously unknown, and no hint was given in synthetic reports on the structure of [OsH₃(PMe₃)₄]⁺.[8] For [RuH₃(PMe₃)₄]⁺, a short T_1 (not minimum) relaxation time suggested that it could contain coordinated H₂, but no further

(12) (a) Saburi, M.; Aoyagi, K.; Takahashi, T.; Uchida, Y. *Chem. Lett.* **1990**, 601. (b) Tsukahara, T.; Kawano, H.; Ishii, Y.; Takahashi, T.; Saburi, M.; Uchida, Y.; Akutagawa, S. *Chem. Lett.* **1988**, 2055. (c) Saburi, M.; Aoyagi, K.; Takeuchi, H.; Takahashi, T.; Uchida, Y. *Chem. Lett.* **1990**, 991. (d) Saburi, M.; Takeuchi, H.; Ogasawara, M.; Tsukahara, T.; Ishii, Y.; Ikariya, T.; Takahashi, T.; Uchida, Y. *J. Organomet. Chem.* **1992**, *428*, 155. (e) Saburi, M.; Aoyagi, K.; Kodama, T.; Takahashi, T.; Uchida, Y.; Kozawa, K.; Uchida, T. *Chem. Lett.* **1990**, 1909. (f) Ogasawara, M.; Aoyagi, K.; Saburi, M. *Organometallics* **1993**, *12*, 3393. (g) Ogasawara, M.; Saburi, M. *J. Organomet. Chem.* **1994**, *482*, 7.

(13) Mezzetti, A.; DelZotto, A.; Rigo, P.; Farnetti, E. *J. Chem. Soc., Dalton Trans.* **1991**, 1525.

(14) Earl, K. A.; Jia, G.; Maltby, P. A.; Morris, R. H. *J. Am. Chem. Soc.* **1991**, *113*, 3027.

(15) Michos, D.; Luo, X.-L.; Crabtree, R. H. *Inorg. Chem.* **1992**, *31*, 4245.

(16) Bampos, N.; Field, L. D. *Inorg. Chem.* **1990**, *29*, 588.

(17) (a) Bianchini, C.; Peruzzini, M.; Zanobini, F. *J. Organomet. Chem.* **1988**, *354*, C19. (b) Eckert, J.; Albinati, A.; White, R. P.; Bianchini, C.; Peruzzini, M. *Inorg. Chem.* **1992**, *31*, 4241. (c) Jia, G.; Drouin, S. D.; Jessop, P. G.; Lough, A. J.; Morris, R. H. *Organometallics* **1993**, *12*, 906. (d) Bianchini, C.; Perez, P. J.; Peruzzini, M.; Zanobini, F.; Vacca, A. *Inorg. Chem.* **1991**, *30*, 279. (e) Bianchini, C.; Linn, K.; Masi, D.; Peruzzini, M.; Polo, A.; Vacca, A.; Zanobini, F. *Inorg. Chem.* **1993**, *32*, 2366. (f) Bautista, M. T.; Earl, K. A.; Maltby, P. A.; Morris, R. H. *J. Am. Chem. Soc.* **1988**, *110*, 4056. (g) Bautista, M. T.; Earl, K. A.; Maltby, P. A.; Morris, R. H.; Schweitzer, C. T. *Can. J. Chem.* **1994**, *72*, 547.

(18) Ogasawara, M. Personal communication.

information was provided.[6] Two papers reported the preparation and reactions of the *phosphite-substituted* [MH(H₂)L₄]⁺ complexes (Table 1). These investigations did not, however, lead to unambigous structural conclusions, although the NMR data presented evidence for the *P structure* of most of them.[5,7]

The analysis of the literature data thus reveals a pronounced preference for the *P* structural type. This seemed to be paralleled by the theoretical results calculated for [RuH₃(PH₃)₄]⁺. The C_n structure derived from the computations on [FeH₃(PH₃)₄]⁺ appeared to be in contradiction with the experiment. Challenged by this, we initially pursued the idea that the small phosphine complexes [FeH₃(PMe₃)₄]⁺ and [RuH₃(PMe₃)₄]⁺ could indeed display different ground state structures in solution. The investigations started on this problem were then naturally extended toward the characterization of [OsH₃(PMe₃)₄]⁺. The choice of monodentate phosphines in these systems was expected to allow maximum degrees of freedom for their structural relaxation around the metal center. It was interesting to see how an increasing steric demand of these substituents could influence this behavior. Therefore, we intended to investigate the structural preferences of the PEt₃ analogues as well.

We sought to apply detailed variable-temperature (VT) NMR studies in conjunction with labeling experiments and with single crystal X-ray investigations in order to get clear insights into the structural and dynamic behavior of the [MH₃L₄]⁺ systems. This report consists of five sections. After a description of the synthetic access to these complexes and their M(H)₂L₄ precursor compounds, the next two sections deliver and discuss the experimental structural findings. The fourth section provides mechanistic studies of the three fluxional processes observed in the [MH₃L₄]⁺ complexes. The final section then deals with the thermodynamic acidity of the cationic molecules and compares the determined pK_a values to those available in the literature for the chelating phosphine analogues [MH(H₂)(dmpe)₂]⁺ and [MH(H₂)(depe)₂]⁺.

II. Synthesis of M(H)₂L₄ and [MH₃L₄]⁺ Complexes (M = Fe, Ru, Os; L = PMe₃, PEt₃)

The *cis*-M(H)₂L₄ derivatives were in most cases the starting materials for our investigation on [MH₃L₄]⁺ complexes. From all of the *cis*-dihydrides of this paper, the syntheses of the PMe₃ derivatives[8a,] and Ru(H)₂(PEt₃)₄[19d] were reported earlier. Due to low yields in some of these preparations and the complicated (multistep) nature of the described approach, decisive modifications of the synthetic procedures had to be developed.

In the Fe(H)₂L₄ series, reduction of FeCl₂ was effected in the presence of excess of L by applying NaBH₄ in ethanol (L = PMe₃, yield 65%). The synthesis of Fe(H)₂(PMe₃)₄ described in a short paper,[8a,19a−c] however, started from LiAlH₄ in THF. The report, unfortunately, did not provide synthetic details.

The synthesis of Fe(H)₂(PEt₃)₄ was achieved *via* the intermediate isolation of Fe(H)₂(N₂)(PEt₃)₃ (yield ca. 70%). This dinitrogen complex was obtained as an oily material slightly contaminated with the spectroscopically identified Fe(H)₂(H₂)(PEt₃)₃ complex (4%) and PEt₃·BH₃ (< 1%). In a subsequent reaction in neat PEt₃, the N₂ and the H₂ ligands of these species could be replaced by the phosphine, which ultimately afforded

(19) (a) Klein, H.-F. *Angew. Chem., Int. Ed. Engl.* **1970**, *9*, 903. (b) Dahlenburg, L.; Frosin, K.-M. *Polyhedron* **1993**, *12*, 427. (c) Behling, T., Girolami, G. S.; Wilkinson, G.; Somerville, R. G.; Hursthouse, M. *J. Chem. Soc., Dalton Trans.* **1984**, 877. (d) Mitsudo, T.; Nakagawa, Y.; Watanabe, K.; Hori, Y.; Misawa, H.; Watanabe, H.; Watanabe, Y. *J. Org. Chem.* **1985**, *50*, 565. (e) Jones, R. A.; Wilkinson, G.; Colquohoun, I. J.; McFarlane, W.; Galas, A. M. R.; Hursthouse, M. B. *J. Chem. Soc., Dalton Trans.* **1980**, 2480.

3718   *J. Am. Chem. Soc., Vol. 119, No. 16, 1997*

Gusev et al.

Table 1. Compilation of the Known $[MH_3L_4]^+$ Complexes (M = Fe, Ru, Os)[a]

L, monodentate	$[FeH(H_2)(PPh(OEt)_2)_4]^+$ (-30, $P + C_n$?[b]);[5] $[FeH(H_2)(P(OEt)_3)_4]^+$ (N/O,[c] C_n?[b]);[5] $[RuH(H_2)(PMe_3)_4]^+$ (N/O,[c] ?[b]);[6] $[RuH(H_2)(PPh(OEt)_2)_4]^+$ (>20, P);[7a] $[RuH(H_2)(P(OEt)_3)_4]^+$ (>-70, P);[7a] $[RuH(H_2)(P(OMe)_3)_4]^+$ (>0, P);[7a] $[OsH_3(PMe_3)_4]^+$ (N/O,[c] ?[b]);[8] $[OsH(H_2)(PPh_2OR)_4]^+$ R = Me (>-70, P), Et (10, P), ^iPr (>-50, P);[7b] $[OsH(H_2)(PPh(OEt)_2)_4]^+$ (>-70, P);[7a] $[OsH(H_2)(P(OEt)_3)_4]^+$ (N/O,[c] P?);[7a] $[Os(H)_3(PPh_3)_4]^+$ (N/O,[c] T)[9]
bidentate	$[FeH(H_2)(dmpe)_2]^+$ (>10, P);[3a,10] $[FeH(H_2)(depe)_2]^+$ (0, P);[3a,11] $[FeH(H_2)(dppe)_2]^+$ (20, P);[2,11] $[FeH(H_2)(dprpe)_2]^+$ (20, P);[3a] $[RuH(H_2)(dmpe)_2]^+$ (>20, P);[3d] $[RuH(H_2)(depe)_2]^+$ (20, P);[11] $[RuH(H_2)(dppe)_2]^+$ (>20, P);[11] $[RuH(H_2)(dppp)_2]^+$ (>20, P);[12a] $[RuH(H_2)(dppb)_2]^+$ (>-10, P);[12a] $[RuH(H_2)(binap)_2]^+$ (>20, P)[12b,g] $[RuH_3(diop)_2]^+$ (>0, $P + T^d$);[12c] $[Ru(H)_3(dppf)_2]^+$ (N/O,[c] T);[12e] $[RuH(H_2)(dpbp)_2]^+$ (-10, T);[12g] $[RuH(H_2)(dcpe)_2]^+$ (20, P);[13] $[OsH(H_2)(dppe)_2]^+$ (>0, P);[14] $[OsH(H_2)(depe)_2]^+$ (-20, P);[14] $[Os(H)_3(dcpe)_2]^+$ (N/O,[c] T)[13]
tridentate + monodentate	$[RuH(H_2)(triphos)(PMe_2Ph)]^+$ (>0, P);[15] $[RuH(H_2)(triphos)(P(OCH_2)_3CEt)]^+$ ($-$, P)[15]
tetradentate	$[FeH(H_2)P(CH_2CH_2CH_2PMe_2)_3]^+$ (N/O,[c] C_n);[16] $[FeH(H_2)P(CH_2CH_2PPh_2)_3]^+$ (10, C_n);[17a,b] $[FeH(H_2)P(CH_2CH_2PCy_2)_3]^+$ (-10, C_n);[17c] $[RuH(H_2)P(CH_2CH_2PPh_2)_3]^+$ (30, C_n);[17d] $[RuH(H_2)P(CH_2CH_2PCy_2)_3]^+$ (0, C_n);[17c] $[OsH(H_2)P(CH_2CH_2PPh_2)_3]^+$ (-80, C_n);[17e] $[Os(H)_3(rac\text{-}tetraphos)]^+$ (N/O,[c] C_c)[17f]; $[Fe,RuH(H_2)(meso\text{-}tetraphos)]^+$ (N/O,[c] P)[17g]

[a] Data in parentheses show the temperature in degrees Celcius of the ^1H NMR decoalescence in the hydride region and the structural assignments as given by the authors. [b] A question mark indicates that the assignment is not reliably established or no structural data are available. [c] Decoalescence was not observed. [d] The second isomer in this mixture was originally thought to be C_n. Subsequent studies proved a trihydride structure, T.[18]

the desired $Fe(H)_2(PEt_3)_4$ product. Both complexes, $Fe(H)_2$-$(PMe_3)_4$ and $Fe(H)_2(PEt_3)_4$, are air sensitive and have to be handled under an inert gas atmosphere. In addition to this, the PMe_3 derivative appeared to be thermally unstable at room temperature and slowly changed from light yellow to dark green in the solid state.

In either case of the reduction with $NaBH_4$, formation of cationic binuclear side-products $\{[(PMe_3)_3Fe]_2(\mu\text{-}H)_3\}^+$ and $\{[(PEt_3)_3Fe(H_2)]_2(\mu\text{-}BH_2)\}^+$ was observed, which were isolated as their $[BPh_4]^-$ salts.
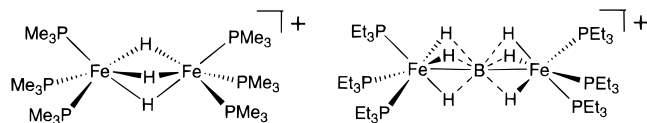
The yield of $\{[(PMe_3)_3Fe]_2(\mu\text{-}H)_3\}[BPh_4]$ seemed to be adjustable at the expense of $Fe(H)_2(PMe_3)_4$, when low stoichiometric amounts of $NaBH_4$ were applied. Both binuclear species were characterized spectroscopically and by single-crystal X-ray diffraction studies. The latter will be published elsewhere. $\{[(PMe_3)_3Fe]_2(\mu\text{-}H)_3\}^+$ possesses a structure of two joint octahedrons which are face-bridged *via* the three hydrogens. The same structural motif has been seen in a related $\{[(PMe_3)_3\text{-}Ru]_2(\mu\text{-}H)_3\}^+$ complex.[19e] The structure of the binuclear PEt_3 derivative can be envisaged to consist of two staggered Fe(II) $[(PEt_3)_3Fe(H)_2]$ units of C_s symmetry which are "held together" by a BH_2^+ cation. In a quite unusual manner, the boron atom thus establishes contacts to all hydride ligands and the iron centers and attains apparent "hypercoordination" in a bicapped octahedral fashion.

The preparation of *cis*-$Ru(H)_2(PMe_3)_4$ was accomplished earlier in a three-step synthesis *via* $RuCl_2(PPh_3)_3$ and $RuCl_2$-$(PMe_3)_4$,[19b] while $Ru(H)_2(PEt_3)_4$ resulted from the direct conversion of $RuCl_3 \cdot nH_2O$ with $NaBH_4$ in the presence of PEt_3,[19d] however in moderate yield. Further explorations on this reaction showed that by the use of the reducing agent $[NBu_4]BH_4$ in THF it was possible to diminish the amount of undesired side-products (such as $RuH_4(PEt_3)_3$) and raise the yield of $Ru(H)_2$-$(PEt_3)_4$ to 76%. This synthetic procedure also allowed a one-pot preparation of $Ru(H)_2(PMe_3)_4$ in 70% yield (eq 1). $Ru(H)_2(PMe_3)_4$ and $Ru(H)_2(PEt_3)_4$ were identified according to their reported NMR spectroscopic properties.[19b,d]

$$RuCl_3 \cdot nH_2O + 4L \xrightarrow[\text{THF}]{[NBu_4]BH_4} cis\text{-}Ru(H)_2L_4 \quad (1)$$

$$L = PMe_3, PEt_3$$
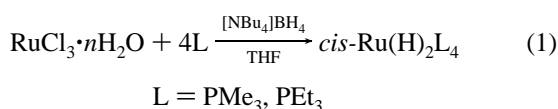
The preparation of $Os(H)_2L_4$ was described for L = PMe_3 by reduction of $OsCl_2(PMe_3)_4$ with sodium naphthalide[8a] or from easily prepared $K_2[OsO_2(OMe)_4]$ and its reaction with PMe_3 in methanol.[19c] In our hands this latter approach was successful with L = PEt_3, but the preparation of $Os(H)_2(PMe_3)_4$ was achieved only after a modification of this synthesis.

An initial ^{31}P NMR spectroscopic pursuit of the transformation of $K_2[OsO_2(OMe)_4]$ and PMe_3 in CH_2Cl_2/CH_3OH (4:1) showed after 1.5 h at room temperature formation of a mixture of the $[Os(CH_3)(PMe_3)_5]^+$ and $[Os(H)(PMe_3)_5]^+$ cations in a 7:3 ratio.[20] In addition to the resonances of these species, a signal of $OPMe_3$ was observed, which indicated that PMe_3 was additionally functioning as a reducing agent. All of these resonances accounted for 90% of the spectrum intensity; however, no dihydride $Os(H)_2(PMe_3)_4$ was observed. When this reaction was attempted in neat ethanol, a similar mixture of $[Os(CH_3)(PMe_3)_5]^+$ and $[Os(H)(PMe_3)_5]^+$ was formed containing ca. 15% of $Os(H)_2(PMe_3)_4$. In both cases, further stirring produced more $[Os(H)(PMe_3)_5]^+$ at the expense of $[Os\text{-}(CH_3)(PMe_3)_5]^+$ (3:2 ratio after 24 h in CH_2Cl_2/CH_3OH).

The original synthetic route was therefore altered to carry out the reaction in ethanol and with $NaBH_4$ as reducing agent, which was applied immediately after addition of the solvent. After 1.5 h at 70 °C the ^{31}P NMR spectrum revealed complete transformation of $[Os(CH_3)(PMe_3)_5]^+$ to $Os(H)_2(PMe_3)_4$, while a small amount of the $[Os(H)(PMe_3)_5]^+$ cation remained unreacted. This reduction presumably involves formation of the neutral complex $Os(PMe_3)_5$, which can lose one phosphine to give $Os(H)(CH_2PMe_2)(PMe_3)_3$.[21] The latter complex has been reported to quantitatively produce the dihydride $Os(H)_2$-$(PMe_3)_4$ in methanol.[8a]

$Os(H)_2(PMe_3)_4$ and $[Os(H)(PMe_3)_5]^+$ were separated by extraction of the former complex with hexane. The dihydride $Os(H)_2(PMe_3)_4$ obtained in this fashion was still contaminated with about 4% of $OsH_4(PMe_3)_3$, but could be used without further purification for the preparation of $[Os(H)_3(PMe_3)_4]^+$.

The reaction of $K_2[OsO_2(OMe)_4]$ with PEt_3 in methanol was also investigated by ^{31}P NMR spectroscopy. After 1 h the resulting clear red solution displayed signals for PEt_3 (-16.8 ppm), $OPEt_3$ (60.9 ppm), $OsH_4(PEt_3)_3$ (1.3 ppm), and two lines at -10.6 and -12.4 ppm corresponding to $[Os(H)_3(PEt_3)_4]^+$ and some reactive intermediate, respectively. Formation of $[Os\text{-}(H)_3(PEt_3)_4]^+$ was completed after 3.5 h. The solution turned almost colorless, and at this point a trace amount of $Os(H)_2$-

(20) (a) $OsMe_2(PMe_3)_4$ is known.[19c] (b) $[OsH(PMe_3)_5]OTf$ has been prepared and characterized.[21]

(21) Ermer, S. P.; Shinomoto, R. S.; Deming, M. A.; Flood, T. C. *Organometallics* **1989**, *8*, 1377.

Table 2. ^{1}H and ^{31}P NMR Spectroscopic Data for the Complexes [MH$_3$(PR$_3$)$_4$]$^+$ Obtained in CDFCl$_2$/CDF$_2$Cl Solutions

[MH$_3$(PR$_3$)$_4$]$^+$	δ(MH)	^2J(H−P)^a Hz (mult.)	T_{1min}, ms	$\delta(^{31}$P)^a (spin system or mulit.)	^2J(P−P), Hz
[FeH(H$_2$)(PMe$_3$)$_4$]$^+$ (**1a**,C_n)	−11.38 (−105°)	br. s (90 Hz)^b	13.5 (−120°)	19.2, 19.8 (A$_2$B$_2$), (−130°)	45.5
[Fe(H)$_3$(PMe$_3$)$_4$]$^+$ (**1a**,T)	−13.28 (−105°)	36 (qi)	196 (−120°)	16.9(d), 31.6 (q), (−130°)	8.0
exchange averaged data^c	−11.68	20.5 (qi)		17.2 (s)	
[Fe(H)$_3$(PEt$_3$)$_4$]$^+$ (**1b**,T)^d	−13.98 (−100°)	non-first-order	177 (−70°)	40.1(d), 67.3 (q)	8.9
exchange averaged data^c	−14.01	39.4 (qi)		46.2 (s)	
[RuH(H$_2$)(PMe$_3$)$_4$]$^+$ (**2a**,C_n)	−8.03 (−130°)	br. s (91 Hz)^b	10.1 (−120°)	−7.2, −8.5 (A$_2$B$_2$), (−50°)	39
exchange averaged data^c	−7.99	br. s (9 Hz)^b		−9.2 (br. s)	
[RuH(H$_2$)(PEt$_3$)$_4$]$^+$ (**2b**,C_n)^d	−8.84 (−90°)^e	br. s (100 Hz)^b		16.0 (t), 21.9 (t)	26.1
[Ru(H)$_3$(PEt$_3$)$_4$]$^+$ (**2b**,T)	−10.33 (−115°)	7.9 (qi/−70°)		17.0 (d), 65.4 (q)	28.9
exchange averaged data^c	−10.10	6.8 (qi)	102 (−50°)^f	26.9 (s)	
[Os(H)$_3$(PMe$_3$)$_4$]$^+$ (**3a**,C_c)	−9.68 (−115°)	±14.6, ∓5.1 (tt)	99.6 (−115°)	−54.5(t), −53.1(t)	18.6
[Os(H)$_3$(PMe$_3$)$_4$]$^+$ (**3a**,T)	−8.87 (−115°)	±10.8 (qi)	207 (−115°)	−50.6 (s)	
exchange averaged data^c	−9.67	±5.2 (qi)		−54.3 (s)	
[Os(H)$_3$(PEt$_3$)$_4$]$^+$ (**3b**,T)	−12.21 (−110°)	15.9 (qi)	194 (−90°)	23.2, −20.2 (AB$_3$), (−130°)	g
exchange averaged data^c	−12.00	15.3 (qi)		−11.4 (s)	

^{a} If not indicated otherwise, the data were obtained at the temperature given in the preceeding column, δ(MH). ^{b} Line width for the broadened single lines. ^{c} All in THF-d_8, at 20 °C. ^{d} In THF-d_8. ^{e} Under these conditions, the chemical shift of **2b**,T is 10.28 ppm. ^{f} Underestimated, because of the exchange with **2b**, C_n. ^{g} Not resolved.

(CO)(PEt$_3$)$_3$ became detectable also. The cation [Os(H)$_3$-(PEt$_3$)$_4$]$^+$ could be precipitated from the reaction solution as a [BPh$_4$]$^-$ salt, however impure, since it cocrystallized with KBPh$_4$. In an alternative treatment evaporation of the reaction solution effected deprotonation of the trihydride to give Os-(H)$_2$(PEt$_3$)$_4$, which was extracted with hexane and converted in a subsequent step into [Os(H)$_3$(PEt$_3$)$_4$]BPh$_4$ by precipitation with a methanol solution of NaBPh$_4$. For the dihydrides Os(H)$_2$L$_4$, we were able to obtain the pure compounds only by deprotonation of [Os(H)$_3$L$_4$]$^+$ with KOH in THF.

The other dihydride complexes of the M(H)$_2$L$_4$ series could also be protonated in methanol. These reactions became complete in a more acidic CH$_3$OH/(CF$_3$)$_2$CHOH mixture. The cationic complexes [MH$_3$L$_4$]$^+$ are readily precipitated as [BPh$_4$]$^-$ salts by the addition of NaBPh$_4$.[16] For X-ray structural characterization the [Fe(H)$_3$(PEt$_3$)$_4$]$^+$ cation has also been obtained as a [B(C$_6$H$_3$(CF$_3$)$_2$)$_4$]$^-$ salt .

III. Stuctural Results: Characterization of the [MH$_3$-(PMe$_3$)$_4$]$^+$ and [MH$_3$(PEt$_3$)$_4$]$^+$ Complexes by NMR and X-ray Complexes by NMR and X-ray

The [MH$_3$L$_4$]$^+$ complexes investigated in this paper are numbered as given below and are eventually additionally denoted to indicate the specific structural isomers (T, C_c, C_n, P; see Scheme 1).

[MH$_3$L$_4$]+	Fe	Ru	Os
PMe$_3$	**1a**	**2a**	**3a**
PEt$_3$	**1b**	**2b**	**3b**

Table 2 lists the most prominent NMR data of the nine [MH$_3$L$_4$]$^+$ isomers traced in our studies. Three solid-state structures (X-ray) will also be reported in this section. However, some of the isomers of [MH$_3$(PR$_3$)$_4$]$^+$ exist only in solution and are not amenable to X-ray determinations. Their structures were solely derived by NMR techniques.

In the [MH$_3$(PR$_3$)$_4$]$^+$ molecules the metal-bound nuclei are magnetically active, and this often permitted unambigous structural assignment based on the interpretation of the ^{1}H and ^{31}P NMR chemical shifts and couplings. Clearly, the T and C geometries can be well distinguished by ^{31}P NMR through the appearance of AB$_3$ *vs* A$_2$B$_2$ spin systems in T *vs* C structures, respectively. The C_c structures are expected to exhibit long relaxation times for the hydrides and hence should display a well-resolved ^{1}H NMR pattern in the hydride region. Fast ^{1}H

relaxation and appreciable broadness are predicted to be characteristic of the C_n isomers.

Other insights can be provided by dynamic NMR. On the basis of coalescence/decoalescence phenomena, it is in many cases possible to evaluate and compare the rates of intramolecular fluxional processes. This work treats the dynamic NMR data as a very important *structurally related* piece of information. When a satisfactory geometry is assigned on the basis of chemical shifts and coupling constants, the structure should as well provide an explanation for the dynamic properties of the molecule.

Facile fluxionality of polyhydride complexes may typically involve significant motions within the H-ligand framework and concomitant minor positional adjustment of the positions of the other hydrides or/and the heavier ligands. It should be recognized that this may lead to averaging of chemical shifts of the heavy ligands as well and therefore pretention of their physical exchange. In other cases these rearrangements are associated with real physical motions of non-hydrogen atoms and molecular subunits. Then, presumably, not too strong topological dispositions are involved. The structural types C, P, and T of Scheme 1 nicely illustrate this concept. It should, however, be pointed out that it may be quite deceptive to assume that a small topological rearrangement of the heavy ligand framework can be concluded from only minor changes in the VT NMR (e.g., ^{31}P NMR) spectra. The fact that no change is observed may simply mean that the chemical shift difference of the averaging nuclei is very small or very large.

Fast phosphorus positional exchange is not feasible in the OsP$_4$ skeleton of the C_n and C_c structures. The known dihydrides *cis*-M(H)$_2$(PR$_3$)$_4$ demonstrate slow or no exchange in their ^{31}P NMR spectra.[1] For instance, Fe(H)$_2$(PMe$_3$)$_4$ and Ru(H)$_2$(PMe$_3$)$_4$ are not fluxional at room temperature.[19a,e] The *cis*-M(H)$_3$ and *cis*-MH(H$_2$) substructures, however, typically show fast hydride or H/H$_2$ scrambling in the reported complexes. This has also been found for all C-type isomers in the present work.

The *trans*-H and -H$_2$ ligands of the P structural type are separated by the ML$_4$ plane. This does not permit fast H/H$_2$ scrambling, and the complexes of this structure quite often display decoalesced H and H$_2$ resonances at ambient temperature. In this case, the ML$_4$ skeleton ought to show a single ^{31}P chemical shift, if the phosphorus ligands are indeed located in one plane. Otherwise, fast ^{31}P fluxionality is expected, since the deviation from the ideal plane should be small and no

substantial motion is required for the exchange between inequivalent positions.

Finally, the *T* type has a single ^{1}H chemical shift and a highly fluxional AB_3 spin system in the ^{31}P NMR. It shall be discussed later in a separate section, how the ^{31}P chemical shift exchange is actually established by *hydride motion* according to the so-called tetrahedral jump mechanism.[1] Following these comments, a detailed characterization of the $[MH_3L_4]^+$ complexes is presented starting with **3b**.

a. Structure of $[OsH_3(PEt_3)_4]^+$ (3b,T). The characterization of the osmium complex **3b** is based on a comparison with the X-ray and NMR data reported for $[Os(H)_3(PPh_3)_4]^+$ (**3c,T**).[9] In the solid state **3c** shows a slightly angularly distorted tetrahedral arrangement of four PPh_3 around the metal (P–Os–P angles, 105° to 114°). Three of the Os–P distances are appreciably longer than the fourth (average 2.473 *vs* 2.290 Å) clearly affected by the *trans*-hydrides (not located) which are presumably all disposed on three of the four tetrahedral faces. The ^{31}P NMR of **3c** shows a "fingerprint" of the *T* structure, two 1:3 resonances (AB_3 spin system). The molecule is fluxional and the two chemical shifts coalesce at −40 °C. At −80 °C, the resonances are still broad and do not exhibit any coupling. A single ^{1}H NMR resonance of the hydrides persists over the whole temperature range studied (22 to −80 °C).

The structure of $[Os(H)_3(PEt_3)_4]^+$ (**3b**) can now easily be derived, since the NMR behavior of this molecule is very similar to that of **3c**. The only substantial difference is that **3b** (with smaller phosphines) is more fluxional. The AB_3 ^{31}P NMR pattern coalesces at −110 °C (the fluxional behavior of all complexes **1**−**3** will be interpreted following the presentation of the structural results). Measurements in a $CDFCl_2/CDF_2Cl$ mixture extended the temperature range to −140 °C, at which end the phosphorus lines did not sharpen enough to reveal any coupling. The hydride resonance of **3b** is a quintet at and above −110 °C. It loses the fine structure below −110 °C, but the expected $ABB'B''XX'X''$ pattern is not yet resolved in the slow exchange regime at −140 °C. The relaxation time T_{1min} is long (194 ms) as expected in the absence of H−H bonding interactions.

The H−D coupling is not resolved at room temperature in the quintet pattern of OsH_2D of the $[OsH_2D(PEt_3)_4]^+$ isotopomer. This monodeuterated derivative of **3b** formed exclusively in CH_3OD solution within 10−15 min preceeding the precipitation as a BPh_4^- salt. The 2.3 Hz $^2J(P-D)$ coupling was resolvable in the exchange-averaged $^{31}P\{^1H\}$ NMR at 20 °C, which permitted the assignment to the $[OsD(H)_2(PEt_3)_4]^+$ structure.

All of these data represent a firm ground for the unambiguous formulation of $[Os(H)_3(PEt_3)_4]^+$ as a classical trihydride (**3b,T**).

b. Structure of $[OsH_3(PMe_3)_4]^+$ (3a,T and 3a,C_c). The solid-state structure of $[Os(H)_3(PMe_3)_4]^+$ is shown in Figure 1 along with selected angles and distances. Different from the PEt_3 analogue, this molecule adopts the *C* geometry. The hydrides were located and refined, but given the high standard deviations in their positions, this does not provide reliable structural information. Solution ^{1}H and ^{31}P NMR experiments were carried out to get more data on the bonding in the OsH_3 fragment.

The solution NMR spectra of $[Os(H)_3(PMe_3)_4]^+$ (Figure 2) show an equilibrium mixture of two isomers. The major component of the mixture (ca. 88% at −115 °C) is one exclusively present in the solid state. In the low-temperature ^{31}P spectra, a characteristic A_2B_2 ($A = P_1, P_3$; $B = P_2, P_4$ according to the numbering of Figure 1) spin system is observed. Fast exchange between the hydride ligands in each isomer

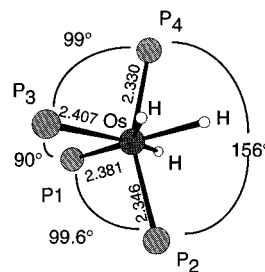**Figure 1.** Structure of the cation in $[Os(H)_3(PMe_3)_4]BPh_4$ with selected angles (deg) and distances (Å) determined by X-ray diffraction. Hydrogen and carbon atoms of the PMe_3 ligands have been omitted for clarity. Additional structural information: Os–H_1 1.57(9); Os–H_2 1.73(11); Os–H_3 1.93(12); H_1–Os–H_2 147(5); H_1–Os–H_3 99(5); H_2–Os–H_3 48(5); H_1–Os–P_1 67(3); H_2–Os–P_3 55(4); P_1–Os–P_4 96.12-(5); P_2–Os–P_3 98.91(5).
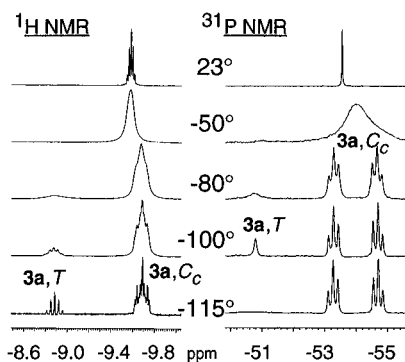
Figure 2. Variable-temperature NMR spectra of $[Os(H)_3(PMe_3)_4]BPh_4$ (**3a**) in $CDFCl_2/CDF_2Cl_2$.

prevents a direct structural assignment even at −140 °C (**3a,C_c** might have shown an XY_2 hydride pattern in the slow-exchange regime). T_1 relaxation time measurements provide an indirect approach.

Long T_{1min} times have been found at −115 °C, well below the decoalescence temperature: 100 and 207 ms for the major and minor isomer, respectively. The 100 ms value can be interpreted in terms of a small contribution to the relaxation from the PMe_3 ligands and either (a) two equal H···H separations, or (b) one short and one long H···H distances.[22] The phosphine contribution has been estimated experimentally in some monohydride octahedral complexes of tungsten and rhenium. The known maximum values are 0.87 s^{-1} in WH-$(CO)_2(NO)(PMe_3)_2$ at −115 °C,[23a] 0.75 s^{-1} in $ReH(CO)_2(PMe_3)_3$ at −106 °C, 1.02 s^{-1} in *cis*-$ReH(CO)(PMe_3)_4$ at −108 °C, and 1.21 s^{-1} in *trans*-$ReH(CO)(PMe_3)_4$ at −101 °C.[23b] For the present calculations, the 1.02 s^{-1} value provided by *cis*-ReH-$(CO)(PMe_3)_4$ seems more appropriate, since this complex adopts a geometry of the phosphorus framework very close to that found in solid **3a**. The case a allows us to estimate that the H···H separation ought to be 1.64(1) Å (∠H−Os−H angle ca. 59°, assuming $r(Os-H) = 1.65$ Å). The model b leads to a short contact of 1.46(1) Å (∠H−Os−H = 52°).

Other Os(IV) trihydrides have a comparable geometry of the $Os(H)_3$ fragment (as calculated from the T_{1min} times): $Os(H)_3$-$Cl(P^iPr_3)_2$ (∠H−Os−H = ca. 58°),[22] $Os(H)_3(\eta^2$-$BH_4)(P^iPr_3)_2$

(22) For an example of these calculations reported for a related trihydride $Os(H)_3Cl(P^iPr_3)_2$ see: Gusev, D. G.; Kuhlman, R.; Sini, G.; Eisenstein, O.; Caulton, K. G. *J. Am. Chem. Soc.* **1994**, *116*, 2685.

(23) (a) Shubina, E. S.; Belkova, N. V.; Krylov, A. N.; Vorontsov, E. V.; Epstein, L.M.; Gusev, D. G.; Niedermann, M.; Berke, H. *J. Am. Chem. Soc.* **1996**, *118*, 1105. (b) Gusev, D. G.; Nietlispach, D.; Vymenits, A. B.; Bakhmutov, V. I.; Berke, H. *Inorg. Chem.* **1993**, *32*, 3270.

(24) Esteruelas, M. A.; Jean, Y.; Lledós, A.; Oro, L. A.; Ruitz, N. Volatron, F. *Inorg. Chem.* **1994**, *33*, 3609.
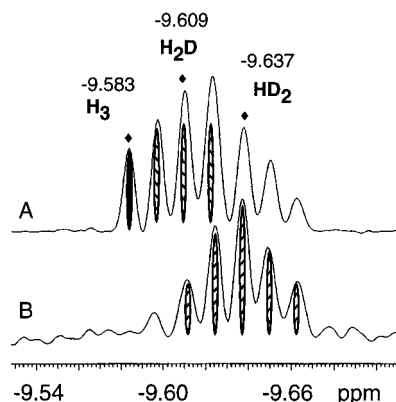
Figure 3. ^{1}H{^{31}P} NMR spectra of the [Os(H,D)$_3$(PMe$_3$)$_4$]BPh$_4$ isotopomers at 20 °C. The OsH$_3$ (singlet), OsH$_2$D (triplet), and OsHD$_2$ (quintet) resonances are shaded. The extent of deuteration increases on going from A to B.

($\angle$H$-$Os$-$H = ca. 60°),[24] and [Os(H)$_3$(NCMe)$_2$(P^{i}Pr$_3$)$_2$]⁺ ($\angle$ H$-$Os$-$H = ca. 57°).[25] All of these complexes show T_{1min} values shorter than in **3a** (72, 82, and 65.5 ms (300 MHz)) because of the larger contribution from the P^{i}Pr$_3$ ligands (estimated as ca. 3.85 s⁻¹). Only Os(H)$_3$Cl(P^{i}Pr$_3$)$_2$ revealed decoalescence in the hydride region of the ^{1}H NMR spectra; the other two examples demonstrated more facile fluxionality.

This consideration indicates that the major isomer is better described as a trihydride with a pentagonal bipyramidal geometry (**3a**,C_c). A helpful comparison is provided by the structure of [Os(H)$_5$(PMe$_2$Ph)$_3$]⁺.[26] The neutron diffraction study of this cation shows a dodecahedral pentahydride that is reminiscent of the molecule in Figure 1 and can formally be generated from **3a**,C_c by replacement of one phosphine by two hydrogens. These new two hydrides would be in the position of either P$_1$ or P$_3$ and split up and down the P$_1$$-Os-P_3$ plane. Finding a coordinated dihydrogen in the presence of four good donors, the PMe$_3$ in **3a** would have been rather inexplicable. Figure 3 shows the isotopically shifted hydride resonances of the [Os(H,D)$_3$(PMe$_3$)$_4$]⁺ isotopomers, which were obtained from the reaction of Os(H)$_2$(PMe$_3$)$_4$ with CH$_3$OD. Phosphorus decoupling clearly reveals a 3.8 Hz H$-$D coupling in [OsH$_2$D-(PMe$_3$)$_4$]⁺ and [OsHD$_2$(PMe$_3$)$_4$]⁺, which is the largest among the other known two-bond couplings in classical hydrides: 3.7 Hz in [CpIr(H)$_3$(AsPh$_3$)]⁺,[27a] 3.3 Hz in Tp*Ir(H)$_4$,[27b] 2.8 Hz in [Os(H)$_3$(NCMe)$_2$(P^{i}Pr$_3$)$_2$]⁺,[25] and 2.4 Hz in [(dippp)Pd]$_2$(μ-H)$_2$.[27c]

The H$-$D couplings in Tp*Ir(H)$_4$, [Os(H)$_3$(NCMe)$_2$(P^{i}Pr$_3$)$_2$]⁺, and [Os(H)$_3$(PMe$_3$)$_4$]⁺ are exchange-averaged ^{av}J(H$-$D), so that their interpretation is model-dependent. For a related example the one-bond H$-$D coupling of a coordinated H$-$D ligand in MH(HD)L$_n$ is three times of ^{av}J(H$-$D).[14] Alternatively, the isotopomers of classical M(H,D)$_3$L$_n$ systems must show an H$-$D coupling between the *cis*-H,D ligands 1.5 times ^{av}J(H$-$D), given that the second H$-$D coupling in this configuration is negligible. From this it is derived to be 5.7 Hz for [Os(H)$_3$(PMe$_3$)$_4$]⁺, if we also neglect that one of the two isomers (e.g., **3a**,T) which may not contribute to the ^{av}J(H$-$D).

The minor isomer of [Os(H)$_3$(PMe$_3$)$_4$]⁺ exhibits a single resonance in the ^{1}H and ^{31}P NMR (Figure 2). The phosphorus

(25) Smith, K.-T.; Tilset, M.; Kuhlman, R.; Caulton, K. G. *J. Am. Chem. Soc.* **1995**, *117*, 9473.

(26) Johnson, T. J.; Albinati, A.; Koetzle, T. F.; Ricci, J.; Eisenstein, O.; Huffman, J. C.; Caulton, K. G. *Inorg. Chem.* **1994**, *33*, 4966.

(27) (a) Computed from the reported ^{2}J(H$-$T) coupling. See: Heinekey, D. M.; Payne, N. G.; Schulte, G. K. *J. Am. Chem. Soc.* **1988**, *110*, 2303. (b) Paneque, M.; Poveda, M. L.; Taboada, S. *J. Am. Chem. Soc.* **1994**, *116*, 4519. (c) Fryzuk, M. D.; Lloyd, B. R.; Clentsmith, G. K. B.; Rettig, S. J. *J. Am. Chem. Soc.* **1994**, *116*, 3804.
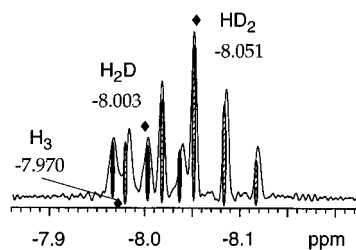

Figure 4. ^{1}H{^{31}P} spectra in the hydride region of the isotopomers of [Ru(H,D)$_3$(PMe$_3$)$_4$]BPh$_4$ in THF-d_8 at 0 °C. The triplet H$_2$D and quintet HD$_2$ are shaded.

spectrum shows line broadening at $-$115 °C, but decoalescence of the resonance was not observed as low as $-$140 °C. The T_{1min} value of 207 ms is longer than the value of 100 ms in **3a**,C_c, presumably because of the longer hydride$-$hydride distances in **3a**,T. Fluxionality is an intrinsic feature of this structural type, and the ^{31}P NMR decoalescence temperature decreases in the order of decreasing bulkiness of the PR$_3$: $-$40 °C (PPh$_3$) > $-$110 °C (PEt$_3$) > ca. $-$140 °C (PMe$_3$).

The variable-temperature ^{1}H NMR data in Figure 2 ($-$140 to +23 °C) indicate very low enthalpy difference ΔH between the isomers. The equilibrium constant K = [**3a**,C_c]/[**3a**,T] shows virtually no temperature dependence below decoalescence (7.4 ($-$100 °C), 6.9 ($-$115 °C), 7.3 ($-$130 °C), and 7.7 ($-$140 °C)). The averaged ^{1}H chemical shift at 23 °C ($-$9.565 ppm in CDFCl$_2$/CDF$_2$Cl) predicts K = 6.2 assuming no temperature dependence for the chemical shifts of the isomers ($-$8.869, **3a**,T and $-$9.676, **3a**,C_c). Molar fractions a and b and their ratio K = a/b can be estimated using the H$-$P couplings at the slow and fast exchange limits. The average coupling is 5.22 Hz at 23 °C. At $-$115 °C the two isomers show H$-$P couplings of $\pm$ 10.80 Hz (quintet of **3a**,T) and $\pm$14.62 per multiplet with a coupling constant of $\mp$5.09 Hz (triplet of triplets of **3a**,C_c). This estimates K as 12.0 at 23 °C. The signs of the couplings follow from the averaging scheme.

These equilibrium data disclose that ΔH is most probably between +0.2 and 0 kcal/mol, while the corresponding ΔS limits are +5.6 eu and +3.9 eu (the latter is $R \ln K$, and K = 7.3, if ΔH = 0). The thermodynamics of the isomerization [**3a**,T] to [**3a**,C_c] is thus almost exclusively governed by the higher entropy of **3a**,C_c.

c. Structure of [RuH(H₂)(PMe₃)₄]⁺ (2a,C_n). Some ^{1}H and ^{31}P NMR parameters have already been reported for the complex [RuH(H$_2$)(PMe$_3$)$_4$]⁺ (**2a**).[6] The present low-temperature mesurements were performed to $-$140 °C. Neither H/H$_2$ decoalescence nor appreciable broadening was observed in the hydride region (singlet at δ $-$8.0, line width 91 Hz at $-$130 °C). The T_{1min} time (10.1 ms, $-$120 °C) represents an average value for the three metal-bound hydrogens, which is characteristic of a dihydrogen complex.

Further information on the structure of **2a** was obtained from deuterium labeling studies. A mixture of the isotopomers of **2a** was prepared from the reaction of Ru(H)$_2$(PMe$_3$)$_4$ with CH$_3$-OD. The ^{1}H{^{31}P} NMR pattern in the hydride region (Figure 4) shows splittings by H$-$D couplings. The magnitude of ^{av}J(H$-$D) is 10.9(1) Hz in the H$_2$D isotopomer *vs* 10.2(1) Hz in the HD$_2$. This indicates a nonstatistical distribution of the isotopes and preferential coordination of the remaining hydrogen as a *hydride*, while deuterium is enriched in the molecular D$_2$ ligand.

From the ^{av}J(H$-$D) values a one-bond H$-$D coupling of 30.6 $-$32.7 Hz can be calculated in the H$-$D ligand of **2a**. No decoalescence was found in the low-temperature ^{1}H NMR spectra of the deuterated **2a** to $-$100 °C in THF-d_8. In addition,
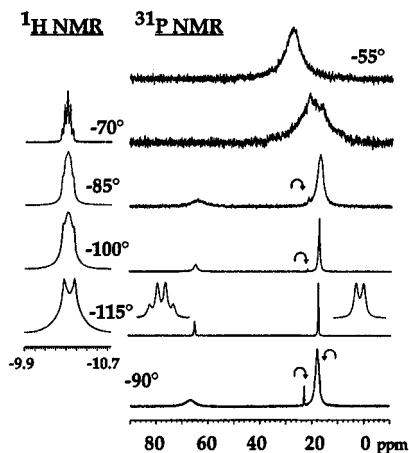
Figure 5. ^1H and ^{31}P NMR spectra of [RuH$_3$(PEt$_3$)$_4$]BPh$_4$ (**2b**) in acetone-d_6 (-90 °C) and a CDF$_2$Cl/CDFCl$_2$ mixture. The larger signals belong to **2b,T**. Arrows indicate the two low-intensity triplets of the **2b,C_n** isomer.

there was no unusual broadening that could signify an isotope effect on the rate of the H/H$_2$ scrambling.

The ^{31}P NMR spectra of [RuH(H$_2$)(PMe$_3$)$_4$]$^+$ show decoalescence at -20 °C. The slow-exchange spectrum displays a well-resolved A$_2$B$_2$ pattern at -50 °C. On the basis of all of these NMR observations [RuH(H$_2$)(PMe$_3$)$_4$]$^+$ (**2a**) must be assigned a C_n structure. Characteristic of the structural types C_n and C_c is a fast exchange between the metal-bound hydrogens, which, however, takes place in a fairly rigid M(PR$_3$)$_4$ skeleton.

d. Structure of [RuH$_3$(PEt$_3$)$_4$]$^+$ (2b,T and 2b,C_n). [RuH$_3$-(PEt$_3$)$_4$]$^+$ (**2b**) is another example of this work, which establishes an equilibrium of two isomers in solution. The major isomer **2b,T** identifies itself by the "fingerprint" NMR data (Figure 5). It shows a well-resolved AB$_3$ ^{31}P spin system (^2J(P−P) = 29 Hz) at -115 °C. This coalesces at -70 °C and is notably less fluxional than that of [Os(H)$_3$(PEt$_3$)$_4$]$^+$. The second isomer of **2b** is present in a very low amount and can be detected in the ^{31}P NMR spectra as an A$_2$B$_2$ spin system (two triplets at -90 °C, Figure 5).

Analyzing the hydride region of the variable-temperature ^1H NMR spectra, one observes a quintet at -10.10 ppm (^2J(H−P) = 6.8 Hz) at 20 °C in THF-d_8. It broadens and loses the fine structure below -10 °C. The maximum broadness (51 Hz) is reached at -50 °C, and subsequent decoalscence brings about two lines at -8.90 and -10.29 ppm at -70 °C. The more intense high-field resonance of **2b,T** appears as a quintet (^2J(H−P) = 7.9 Hz) at -70 °C in CDFCl$_2$/CDF$_2$Cl. In neither of the three solvents employed here (THF, acetone, and the CDFCl$_2$/CDF$_2$Cl mixture) the low-intensity resonance at -8.9 showed further decoalescence. In addition to this, the line was persistently broad and did not show any coupling to the ^{31}P nuclei. These spectroscopic properties suggest a C_n structure for the minor isomer. It is assumed to be a dihydrogen complex [RuH(H$_2$)(PEt$_3$)$_4$]$^+$ by analogy with the PMe$_3$ derivative. The direct observation of an expected large J(H−D) coupling or a short T_{1min} time was not possible for **2b,C_n** due to the unfavorable equilibrium situation.

At -70 °C the hydride resonance of **2b,T** transforms from an exchange-averaged quintet into a complicated pattern of an ABB′B″XX′X″ spin system at -115 °C (Figure 5). A T_{1min} relaxation time of 102 ms was measured for the hydride ligands at -50 °C. At this temperature the equilibrium is fast on the NMR time scale, which causes the relaxation time to be averaged for the two isomers. It is mainly determined by the
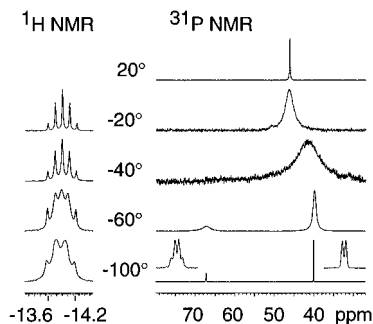

Figure 6. Variable-temperature ^1H and ^{31}P NMR spectra of [Fe(H)$_3$-(PEt$_3$)$_4$][B(C$_6$H$_3$(CF$_3$)$_2$)$_4$] in THF-d_8.
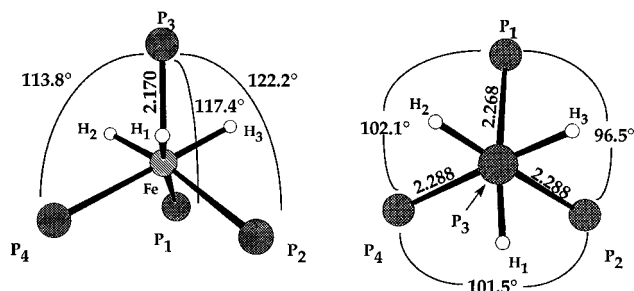
Figure 7. The structure of [Fe(H)$_3$(PEt$_3$)$_4$][B(C$_6$H$_3$(CF$_3$)$_2$)$_4$] (**1b,T**) with selected angles (deg) and distances (Å) determined by X-ray diffraction. Hydrogen and carbon atoms of the PEt$_3$ ligands have been omitted for clarity. Additional data: Fe−H (av) = 1.44(7) Å, P$_3$−Fe−H (av) = 67(3), P$_{1,2,4}$−Fe−H (av) = 77(3), 173°(3).

contribution of **2b,T**, since the second isomer is present in a very low amount only. It is noteworthy, that the equilibrium constant [**2b,T**]/[**2b,C_n**] increases when the solvent polaritiy decreases: 22 (acetone-d_6) < 32 (THF-d_8) < ca. 55 (CDFCl$_2$/CDF$_2$Cl) at -90 °C.

The pair of ruthenium complexes **2a** and **2b** corroborate the trend already shown by the osmium molecules **3a** and **3b**: for each metal the heavier PEt$_3$ congeners prefer the arrangement which allows maximum relief of steric strain. This is the T type structure, where the phosphorus ligands are pseudotetrahedrally arranged around the metals. The ruthenium system is indeed driven by the sterics to adopt the high +IV formal oxidation state in **2b,T**, which otherwise is only rarely found within the realm of ruthenium hydrides.[28]

e. Structure of [Fe(H)$_3$(PEt$_3$)$_4$]$^+$ (1b,T). This molecule is the most representative example of the T structural type characterized within this work. Species **1b,T** is the only isomer present. It shows the fingerprint of an AB$_3$ ^{31}P spin system, which is moderately fluxional and sharpens nicely at -100 °C, the lowest temperature attainable in THF-d_8 (Figure 6). The decoalescence temperature is about -40 °C and reveals another trend for the T geometry: the lighter metal congeners are more rigid in the Fe−Ru−Os triad.

A high-temperature quintet resonance of Fe(H)$_3$ exhibits changes on lowering the temperature to give a complicated pattern of an ABB′B″XX′X″ spin system in the slow-exchange regime. The relaxation time T_{1min} = 177 ms rules out any bonding interaction between the hydrides.

The molecular structure of **1b,T** is shown in Figure 7. The coordination around the iron atom can be envisaged as a distorted FeP$_4$ tetrahedron capped by the three terminal hydrogen atoms on three of the trigonal faces. Alternatively this molecule can be assembled from an octahedral *fac*-[Fe(H)$_3$(PEt$_3$)$_3$]$^+$

(28) (a) Chinn, M. S.; Heinekey, D. M. *J. Am. Chem. Soc.* **1990**, *112*, 5166. (b) Jia, G.; Morris, R. H. *J. Am. Chem. Soc.* **1991**, *113*, 875. (c) Jia, G.; Lough, A. J.; Morris, R. H. *Organometallics* **1992**, *11*, 161.
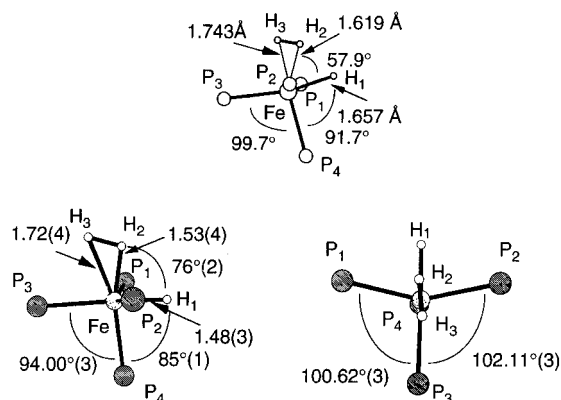
M(II) and M(IV) Complexes [MH₃(PR₃)₄]⁺

J. Am. Chem. Soc., Vol. 119, No. 16, 1997 3723

Figure 8. Comparison of the structural data provided by an *ab initio* calculation[4a] on [FeH(H₂)(PH₃)₄]⁺ (top) and the X-ray diffraction of [FeH(H₂)(PMe₃)₄]BPh₄ (two views below). Other selected distances (Å) and angles (deg): H₂–H₃ 0.84(4), Fe–P₁ 2.230(1), Fe–P₂ 2.231(1), Fe–P₃ 2.260(1), Fe–P₄ 2.212(1), H₂–Fe–H₃ 32(2), P₁–Fe–P₂ 152.51-(3), P₁–Fe–P₄ 95.59(3), P₂–Fe–P₄ 98.05(3).

Figure 9. Low-temperature ^{31}P NMR spectra of the two isomers of [FeH₃(PMe₃)₄]BPh₄ in a CDFCl₂/CDF₂Cl mixture.

fragment and a PEt₃ cap on the face of the three hydrogens. This fourth phosphorus ligand is indeed located on an idealized 3-fold axis of symmetry. Since there is no *trans*-ligand for that phosphorus moiety, the Fe–P bond is rather short, 2.170(2) Å, while the other three Fe–P distances are elongated to 2.268–2.288(2) Å because of the strong *trans*-influence of the hydrides. Similar features can be seen in the other two solid-state structures of the *T* type, [Ru(H)₃(dppf)₂]⁺ (2.325 *vs* av 2.416 Å)[12d] and [Os(H)₃(PPh₃)₄]⁺ (2.290 *vs* av 2.473 Å).[9] Quite naturally, the Fe–P bonds are 5–8% shorter than the corresponding Ru–P and Os–P ones and the ligand arrangement is more compact (compressed) in [Fe(H)₃(PEt₃)₄]⁺.

The formal +IV oxidation state in [Fe(H)₃(PEt₃)₄]⁺ is unusual for iron hydrides. The other reliably established Fe(IV) hydride systems are the cationic [Cp*Fe(dppe)(H)₂]⁺[29a] and the neutral (η⁶-arene)Fe(H)₂(SiCl₃)₂ complexes.[29b] For the hydrido silyl and stannyl complexes FeH₃(PPh₂R′)₃ER₃ (ER₃ = SnPh₃ (R′ = ⁿBu), SiMePh₂ (R′ = ⁿBu), SnPh₃ (R′ = Et)), the same structure is assumed on spectroscopic grounds, however, definite structural conclusions were not given.[29c] The C_3 symmetric heavy atom skeleton of FeH₃(PPh₂Et)₃(SnPh₃) is reminiscent of the Fe(PEt₃)₄ fragment (Fe–P: 2.239 Å (average) and P-Fe-Sn: 113.7°,114.0°, 118.7°). The metal-bound hydrogens were not located. The reported spectroscopic data indicated the possibility of an additional E-H secondary type bonding.

f. Structure of [FeH₃(PMe₃)₄]⁺ (1a,*T* and 1a, C_n). The X-ray structure analysis of [FeH₃(PMe₃)₄]⁺ reveals a distorted octahedral geometry **1a**,C_n around the iron center (Figure 8). The three metal-bound hydrogens were located as a *cis*-disposed hydride and a dihydrogen ligand. The two equatorial phosphines P₃ and P₄ show different distances to iron: longer (2.260 Å, P₃) when *trans* to H and shorter (2.212 Å, P₄) when *trans* to dihydrogen. Both bond lengths are in the range of Fe–P distances observed in the [Fe(H)₃(PEt₃)₄]⁺ cation: (2.28 Å (*trans* to H, av) to 2.17 Å (*trans* to an empty coordination site).

The geometries of the experimental and calculated structures of Figure 8 compare well. They demonstrate a reasonable agreement between most of the angles and distances. Some substantial disparity in Figure 8 is evident only in the iron to

(29) (a) Hamon, P.; Toupet, L.; Hamon, J.-R.; Lapinte, C. *Organometallics* **1992**, *11*, 1429. (b) Yao, Z.; Klabunde, K. J.; Asirvatham, A. S. *Inorg. Chem.* **1995**, *34*, 5289. (c) Schubert, U.; Gilbert, S.; Mock, S. *Chem. Ber.* **1992**, *125*, 835.

(30) Van Der Sluys, L. S.; Eckert, J.; Eisenstein, O.; Hall, J. H.; Huffman, J. C.; Jackson, S. A.; Koetzle, T. F.; Kubas, G. J.; Vergamini, P. J.; Caulton, K. G. *J. Am. Chem. Soc.* **1990**, *112*, 4831.
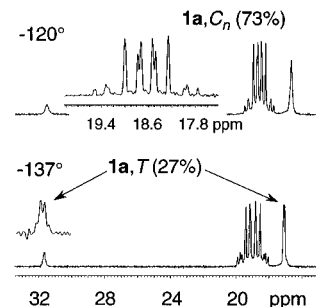
hydrogen bonds. They are shorter in the experimental structure (Fe–H 1.48 Å, Fe(H₂) 1.53 and 1.72 Å) and are in a better agreement with the neutron diffraction data available for the related Fe(H)₂(H₂)(PEtPh₂)₃ molecule.[30] The latter shows two Fe–H distances of 1.514 Å (*trans* to PEtPh₂) and 1.538 Å (*trans* to coordinated dihydrogen) and two distances in the Fe(H₂) fragment (1.576 and 1.607 Å). There is a remarkable asymmetry of bonding in the Fe(H₂) demonstrated by all three (calculated and experimental) structures. This was explained invoking a weak attractive interaction between the *cis*-H and -H₂ ligands (between H₁ and H₂ in Figure 8). The theoretical report on [FeH(H₂)(PH₃)₄]⁺ also mentions that those hydrogens in the positions of H₃ and H₂ look as if they retained "memory" on their chemical origin, i.e., that one of H₃ appears as a proton coordinating onto a classical hydride–iron bond.[4a] This structural feature however still remains speculative without neutron diffraction data for [FeH(H₂)(PMe₃)₄]⁺.

In solution, a fast equilibrium is established between the *two isomers* of **1a** (Figure 9). The rate of equilibration becomes slow on the NMR time scale below −80 °C. Resonances for the solid-state isomer **1a**,C_n can then be identified. In the ^{31}P NMR, they give rise to a characteristic A₂B₂ pattern. The second isomer appears as an AB₃ spin system, which confirms an **1a**,*T* structural assignment (Figure 9). The **1a**,*T* is more fluxional than **1b**,*T* bearing *larger phosphines*. The former displays resolved ^{31}P–^{31}P coupling at −137 °C, while the latter complex shows this at −100 °C.

As expected from the ^{31}P NMR investigations, the hydride region of the ¹H NMR spectrum reveals resonances for **1a**,C_n and **1a**,*T* below the decoalescence temperature of −80 °C. A single broad line of the metal-bound hydrogens of **1a**,C_n, present even at −140 °C, indicates a typical very fast H/H₂ scrambling. The hydride resonance of **1a**,*T* is a quintet (ᵃᵛJ(H−P) = 36 Hz) at −105 °C. When the temperature is lowered, it shows a transformation quite similar to that given by [Fe(H)₃(PEt₃)₄]⁺ in Figure 6. The central lines of the quintet broaden, and then the quintet decoalesces into a multiplet, which may remind one of a triplet of doublets at −130 °C. The doublet feature (38 Hz) proved to be the ²J(H−P_A) coupling by selective decoupling at the B₃ ^{31}P chemical shift.

The T_{1min} relaxation times were reached at −120 °C. They are characteristically short (13.5 ms) for the averaged FeH(H₂) line of **1a**,C_n and long (196 ms) for the classical hydride resonance of **1a**,*T*.

A deuterated derivative of **1a** was prepared by the reaction of Fe(H)₂(PMe₃)₄ with CH₃OD precipitated as a BPh₄⁻ salt. A freshly prepared (1 h after isolation of the solid) and strongly D-enriched sample of **1a** shows a residual HD₂ quintet resonance at δ −11.651 in the ¹H{^{31}P} NMR (ᵃᵛJ(H−D) = 8.1(1) Hz at 20 °C in CD₂Cl₂). This solid material changed and revealed a decreased amount of metal-bound deuterium after 6 h of storage at 20 °C. The ¹H{^{31}P} NMR spectrum then showed a mixture

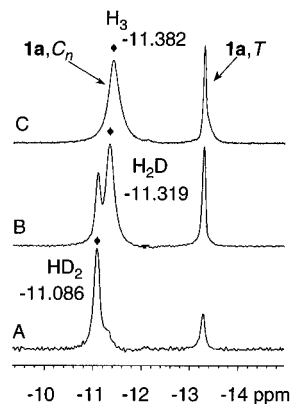**Figure 10.** $^1H\{^{31}P\}$ NMR spectra of the isotopomers of [Fe(H,D)$_3$-(PMe$_3$)$_4$]BPh$_4$ recorded in a CDFCl$_2$/CDF$_2$Cl mixture at -130 °C. The spectra A, B, and C differ in the deuterium content. They were obtained by the isomerization of a fully deuterated solid sample of **1a** (A after 1 h, B after 12 h, and C after 24 h).

of the HD$_2$, H$_2$D isotopomers (triplet at δ -11.730, $^{av}J(H-D)$ = 8.6(1) Hz) and the perprotio complex (singlet at δ -11.758). Finally, after 24 h at 20 °C, the crystalline material turned out to be mostly FeH$_3$. The ^2H NMR of this solid dissolved in CH$_3$CN demonstrated that methyl groups of the PMe$_3$ ligands were randomly deuterated: three 2:1:1 resonances of a newly formed and stereochemically rigid [FeH(CH$_3$CN)(P(Me-d)$_3$)$_4$]$^+$ molecule could be resolved.

This remarkable intramolecular H/D exchange, which takes place in the *solid state*, is unprecedented among dihydrogen complexes. It appears that mechanistically it requires replacement of the D$_2$ (or HD) ligand by an agostic C$-$H bond, activation of the C$-$H bond and ultimately Fe$-$D/C$-$H scrambling. If this happens relatively fast and in a reversible fashion, the D$_2$ trapped in the lattice is expected to regenerate the starting material. An agostic interaction of this type was reported in the 16 electron complexes [RuH(P$-$P)$_2$]PF$_6$ (bidentate phosphine P$-$P = dppb and diop) where the agostic hydrogen was in exchange with the terminal hydride.[12f] A related example of unusual H/D exchange is known for the Kubas complex W(H$_2$)(CO)$_3$(P^{i}Pr$_3$)$_2$, where W(D$_2$)(CO)$_3$(P^{i}Pr$_3$)$_2$ is formed under D$_2$ also in solid state. However, the mechanism of this process is not yet fully established.[31]

The isotopomers of **1a**,C_n demonstrate peculiar isotope effects at low temperature. The three $^1H\{^{31}P\}$ NMR spectra in Figure 10 differ in the relative D/H isotopomeric contents. The sample of **1a**,C_n with a maximum degree of deuteration (spectrum A) almost exclusively consists of the HD$_2$ isotopomer. Its $^1H\{^{31}P\}$ NMR resonance is significantly shifted down-field with respect to both the H$_2$D and H$_3$ signals. Because of this difference in the chemical shifts, two resolved resonances of approximately 1:2 intensity can be observed for a less D-enriched sample of **1a**,C_n (spectrum B) and thus can mistakenly be interpreted as an H/H$_2$ decoalescence. The H$_3$ resonance of spectrum C in Figure 10 is broad, apparently because of the strong H$-$H dipole interactions. It sharpens upon deuteration, but the expected H$-$D coupling of $10-11$ Hz could still not be resolved.

Another peculiar isotope effect is observed in the low-temperature ^{31}P NMR spectra of the deuterated classical complex **1a**,T. The axial PMe$_3$ ligand, which appears strongly shifted low-field (Figure 9, δ 31.68 at -130 °C), shows pronounced isotope shifts: δ 32.25 (DH$_2$), 32.82 (D$_2$H), and 33.38 (D$_3$). The total change $\Delta\delta(^{31}P)$ between the Fe(H)$_3$ and Fe(D)$_3$ isotopomers is unusually large for a secondary isotope effect: 1.7 ppm. This can be explained by the unique structural

Scheme 2

C_c and C_n ⟶ T
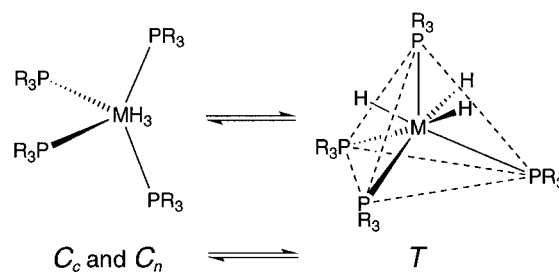
position of this ligand which is "surrounded" by all three hydrides in [Fe(H)$_3$(PMe$_3$)$_4$]$^+$.

In the spectra of Figures 9 and 10 it can be seen that **1a**,C_n is the major isomer in solution. The equilibrium constant K = [**1a**,C_n]/[**1a**,T] is solvent-dependent and increases with increasing polarity: 2.7 (CDFCl$_2$/CDF$_2$Cl) < 4.0 (CD$_2$Cl$_2$) < 6.7 (acetone-d_6) (all between -100 and -110 °C). In the CD$_2$Cl$_2$ case, it appears that K = 4 does not change appreciably between -100 and $+20$ °C. However, fast exchange does not permit a direct measurement of K above -90 °C; it can be estimated on the basis of $^{av}J(H-D)$ = 8.1 (in HD$_2$) to 8.6 Hz (in H$_2$D) at 20 °C. A related complex of the C_n structure [FeH(H$_2$)P(CH$_2$CH$_2$CH$_2$-PMe$_2$)$_3$]$^+$ shows $^{av}J(H-D)$ = 10 (in HD$_2$) to 11 Hz (in H$_2$D).[16] Assuming a negligible H$-$D coupling in the classical isomer **1a**,T, allows to estimate its relative contribution between $19-$22% and a K of 3.6$-$4.3 at 20 °C. In agreement with this, the averaged chemical shift of FeH$_3$ does not show any temperature dependence between 20 and -60 °C.

Most probably the two isomers **1a**,C_n and **1a**,T have the same enthalpy and $\Delta H°$ = 0. The thermodynamic situation in CD$_2$-Cl$_2$ is then governed only by the entropy difference which obviously is $\Delta S°$ = R ln K = ca. 3 eu. This small entropy change is indeed associated with the thermodynamics of a classical dihydride to dihydrogen complex transformation. It is explained by the loss of the spinning degree of freedom of the dihydrogen ligand.[32]

IV. Discussion of the Structural Results for the Complexes 1$-$3

The [$C \rightleftharpoons T$] isomerization illustrated in Scheme 2 is the major structural theme, one is persistently encountering, reviewing the structure of the [MH$_3$(PR$_3$)$_4$]$^+$ cations **1**$-$**3**. Both types of isomers are formed in solutions of [FeH$_3$(PMe$_3$)$_4$]$^+$, [RuH$_3$-(PEt$_3$)$_4$]$^+$, and [OsH$_3$(PMe$_3$)$_4$]$^+$. Two complexes are completely on the right side of the [$C \rightleftharpoons T$] equilibrium: [Fe(H)$_3$(PEt$_3$)$_4$]$^+$ and [Os(H)$_3$(PEt$_3$)$_4$]$^+$. [RuH(H$_2$)(PMe$_3$)$_4$]$^+$ exclusively exist as C_n isomers.

The different steric bulk of PMe$_3$ and PEt$_3$ is an apparent structural characteristic that significantly influences the [$C \rightleftharpoons T$] equilibrium (the electronic properties of these ligands are similar). The C type is destabilized by more bulky PEt$_3$ ligands, which prefer a tetrahedral arrangement around the metal. Another important circumstance is that the [$C \rightleftharpoons T$] transformation changes the formal oxidation state of M(II) to M(IV). This represents a crucial factor for ruthenium and iron, which are difficult to oxidize and strongly favor the oxidation state +II.

[OsH$_3$(PMe$_3$)$_4$]$^+$ shows little preference for **3a**,C_c over **3a**,T, and both are classical hydrides. [RuH(H$_2$)(PMe$_3$)$_4$]$^+$ can only exist as a dihydrogen complex **2a**,C_n. Note, that the M$-$P bonds are actually shorter in ruthenium complexes and make the interligand repulsions stronger than in the isostructural osmium molecules. Even the additional steric bulk introduced by PEt$_3$

(31) Kubas, G. *J. Acc. Chem. Res.* **1988**, *21*, 129.

(32) Jessop, P. G.; Morris, R. H. *Coord. Chem. Rev.* **1992**, *121*, 155.

in $[RuH_3(PEt_3)_4]^+$ did not impose a strong enough driving force to shift the $[C \rightleftarrows T]$ equilibrium completely to the right.

The equilibrium behavior of both the PMe_3 and PEt_3 iron molecules, i.e., a relatively high stability of **1a**,*T* and **1b**,*T*, is unexpectedly more reminiscent of that shown by the osmium rather than ruthenium systems. This is indeed counterintuitive and violates the normal periodic trend. Some contraction of the M–P bond distances on going from ruthenium to iron could, in principle, cause some destabilization of **1a**,C_n and **1b**,C_n. A comparison provided by the available X-ray data of *cis*-[FeH-$(H_2)(PMe_3)_4]^+$ and *cis*-Ru(H)₂(PMe₃)₄,[19b] however, does not reveal a drastic difference: 2.260 (Fe–P) *vs* 2.306 Å (Ru–P) (*trans* P–M–H) and 2.230 (Fe–P) *vs* 2.276 and 2.289 Å (Ru–P) (*trans* P–M–P).

In searching for an explanation of this phenomenon, some other chemical and spectroscopic properties of complexes **1a** and **2a** are expected to be relevant here. The first is that the T_{1min} relaxation time is longer in $[FeH(H_2)(PMe_3)_4]^+$ (13.5 ms) than in $[RuH(H_2)(PMe_3)_4]^+$ (10.1 ms). This indicates a longer H–H bond (i.e., more activated dihydrogen ligand) in **1a**,C_n. Coordinated H_2 appears to be more labile in $[RuH(H_2)(PMe_3)_4]^+$. It loses H_2 reversibly, and both dissolved H_2 and RuH₃ resonances are noticeably broad at 20 °C. The reactivity of $[RuH(PMe_3)_4]^+$ has been reported,[33,34] and the five-coordinate complexes of bidentate dppe, dppp,[12a] binap,[12b] dppb,[12a,f] and diop[12c,d,f] ligands, $[RuH(P–P)_2]^+$, have been characterized.

The corresponding iron molecular fragment $[FeH(PMe_3)_4]^+$ presumably cannot be isolated. It is this intermediate which should be responsible for the C–H bond activation and the H/D scrambling observed in the deuterated solid **1a**. The deuterated ruthenium complex **2a** does not exchange methyl hydrogens for the metal-bound deuterons, i.e., the ruthenium fragment $[RuH(PMe_3)_4]^+$ is less reactive toward C–H oxidative addition.

We believe that the higher tendency of **1a** and **1b** (in comparison with the ruthenium representatives **2a** and **2b**) to adopt a trihydride *T* structure is driven by electronic rather than steric factors. Previous reports on *trans*-$[MH(H_2)(P–P)_2]^+$ with chelating phosphines already indicated that[3c] "...the dihydrogen ligand is activated toward homolytic cleavage the most in the osmium complexes and the least in the ruthenium complexes, with the iron complexes being intermediate in nature". The present findings in the isomeric *cis*-$[MH(H_2)(PMe_3)_4]^+$ systems corroborate this trend.

In a different series of the type $[Cp^*M(P–P)H_2]^+$, the only known iron complex (P–P = dppe) is a Fe(IV) dihydride in solution.[29a] The ruthenium analogue has not been reported, but the related $[CpRu(dppe)H_2]^+$,[28b] $[Cp^*Ru(dmdppe)H_2]^+$,[28a] and $[Cp^*Ru(dppm)H_2]^+$[28b,c] complexes show equilibrium mixtures of the dihydride and dihydrogen isomers. $[Cp^*Ru(dppp)H_2]^+$ is a dihydride in solution at 20 °C.[28b] This comparison also shows that the ability of iron toward oxidative additon of H_2 is (at least) not lower than that of ruthenium.

It has already been mentioned in the introduction (Table 1) that the *phosphite* and *phosphonite* complexes $[MH(H_2)P_4]^+$ (M = Fe, P = PPh(OEt)₂; M = Ru, P = PPh(OEt)₂, P(OEt)₃, P(OMe)₃) display spectroscopic properties consistent with a *P* structure.[5,7] The metal centers of these molecules are certainly less electron-rich than those of the *phosphine* complexes in this work. For this reason formation of any phosphite trihydride is expected to be electronically less favorable.

The results of this work demonstrate that a reliable theoretical evaluation of the $[MH_3L_4]^+$ complexes should take into account both steric and electronic properties of the ligands L. The maximum number of different isomers *four* is represented in the osmium system, while the ruthenium and iron molecules show *three* isomeric types (Table 1). For any computational work dealing with such metal complexes containing three or four phosphorus ligands, it is therefore desirable to consider all conceivable structural possibilities. Since the structural preference of these complex systems is highly dependent on the stereoelectronic properties of the phosphine ligands, one should be prepared to find modified and even altered relative energies of the isomers, when the bulkiness and donicity of the PR_3 ligands significantly differ from those of the widely used theoretical model ligand PH_3.

V. Mechanism of Isomerization and Ligand Exchange in $[MH_3(PR_3)_4]^+$

a. Very Fast H/H₂ Scrambling. Three dynamic processes influence the NMR spectra of the $[MH_3(PR_3)_4]^+$ complexes. One is the H/H₂ scrambling in **1a**,C_n, **2a**,C_n, and **2b**,C_n of the type which has been thoroughly analyzed theoretically.[4b] A reasonable mechanism for this exchange has been named "open direct transfer". It requires elongation of the H–H bond with concomitant shortening of the separation between the hydride and the contiguous hydrogen of the H_2. Both H···H distances become equal and relatively short in the transition state. Fast H_2 spinning in the ground-state structure completes the site exchange.

The examples of this work and others from the literature show that *cis* H and H_2 ligands are as a rule engaged in very fast exchange when decoalescence cannot be reached in low-temperature ¹H NMR experiments. The only notable exception is represented by the complexes $[MH(H_2)L_4]^+$ with *tetradentate* phosphorus ligands $L_4 = PP_3$ (Table 1), which have H/H₂ decoalescence temperatures as high as 30 °C. This exceptional behavior has never been discussed and is far from being understood. This group, however, may have a structure of a capped trigonal bipyramid, where the hydride resides on a P–P–P face and is thus separated from the H_2 ligand by a P–P edge.

cis-Trihydrides exchange metal-bound hydrogens by a pairwise "replacement" mechanism, which was extensively analyzed by computational methods.[35] On the way to the transition structure, two neighboring hydrides swing up and down, off the ground-state M(H)₃ plane. The H···H vector shortens and becomes perpendicular to the plane in the transition structure. Exchange of this type has been studied experimentally in a number of trihydrides, which all showed facile fluxionality. The trihydride $[Os(H)_3(PMe_3)_4]^+$ (**3a**,C_c) did not reveal decoalescence in the hydride region even at −140 °C. In addition to this, no deuterium isotope effect was noticeable for this process in the deuterated complex of **3a**. Apparently, in the presence of small phosphine ligands the height of the barrier for the site exchange in $[Os(H)_3(PMe_3)_4]^+$ can be relatively low.

b. "Tetrahedral Jump" Hydride Reorientation in the T Structure. The *T* type complexes $[Fe(H)_3(PMe_3)_4]^+$, $[Fe(H)_3(PEt_3)_4]^+$, $[Ru(H)_3(PEt_3)_4]^+$, $[Os(H)_3(PMe_3)_4]^+$, and $[Os(H)_3(PEt_3)_4]^+$ are nonrigid, and the four phosphorus atoms appear magnetically equivalent at 20 °C. When the temperature is lowered, the characteristic AB₃ spectra could be observed in the ³¹P NMR. The rate of the fluxional process responsible for averaging of the ³¹P chemical shifts shows pronounced dependence on the size of the phosphines and metal. It increases in

(33) (a) Rappert, T.; Yamamoto, A. *Chem. Lett.* **1994**, 2211. (b) Burn, M. J.; Bergman, R. G. *J. Organomet. Chem.* **1994**, *472*, 43.

(34) Rappert, T.; Yamamoto, A. *Organometallics* **1994**, *13*, 4984.

(35) (a) Jarid, A.; Moreno, M.; Lledós, A.; Lluch, J. M.; Bertrán, J. *J. Am. Chem. Soc.* **1995**, *117*, 1069. (b) Clot, E.; Leforestier, C.; Eisenstein, O.; Pélissier, M. *J. Am. Chem. Soc.* **1995**, *117*, 1797.
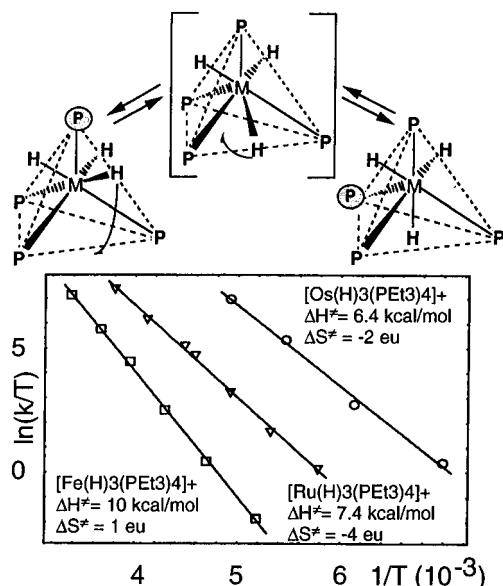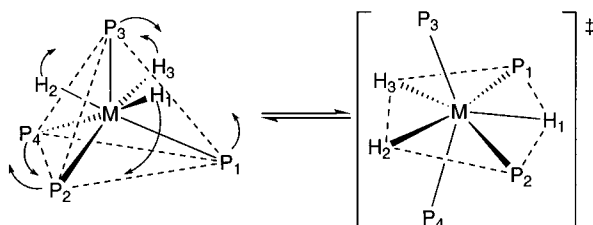
Figure 11. A schematic representation of the "tetrahedral jump" hydride reorientation in the T type structure and Eyring plot of the rate constants of this process in $[Fe(H)_3(PEt_3)_4]^+$, $[Ru(H)_3(PEt_3)_4]^+$, and $[Os(H)_3(PEt_3)_4]^+$ derived from the variable-temperature ^{31}P NMR spectra using the DNMR5 program. Determined activation enthalpies and entropies are given in the plot.

Scheme 3

the order: Fe < Ru < Os (Figure 11) and PPh_3 < PEt_3 < PMe_3. $[Os(H)_3(PMe_3)_4]^+$ shows the fastest rate, and the slow exchange regime could not be attained even at -140 °C. A barrier for the rearrangement in this molecule must be lower than 6.4 kcal/mol determined for $[Os(H)_3(PEt_3)_4]^+$ by analysis of the variable temperature ^{31}P NMR data with the DNMR5 program (Figure 11). For $[Fe(H)_3(PMe_3)_4]^+$ a rough estimate for the barrier is $\Delta G^{\ddagger} = 7.8(1)$ kcal/mol between -100 and -120 °C.

A mechanism assuming *hydride migration* as a key step (principal motion) provides a reasonable explanation for the very fast fluxionality and the experimental observations. Given in Figure 11, it involves the passage of one hydride from its face to a vacant one *via* the tetrahedral edge of the MP_4 skeleton (tetrahedral jump). In the ^{31}P NMR the chemical shifts are altered in a pairwise fashion. Figure 11 shows how the environments of two phosphorus atoms (shaded before and after the jump) are interchanged in a single event of exchange. The rate constants determined in Figure 11 from the ^{31}P NMR spectra thus describe the rate of the *hydride* face-to-face migration. More strictly, they represent the lifetime of the empty site of the tetrahedron.

Certain secondary topological modifications of the skeleton are required to lower the barrier for the hydride migration. Indicated in Scheme 3: both P_1–M–P_2 and P_3–M–P_4 angles should open up - one to permit the passage of the hydride, the other to accomodate the hydrogens H_2 and H_3, which are moving toward each other and away from P_1 and P_2. The transition geometry presumably has a shape of a distorted pentagonal bipyramid.

A number of factors would determine the energy of the transition state. An obvious one is the crowding in the P–M–P edge region. There is a clear correlation in the experimental data: the larger the steric bulk of PR_3, the higher the barrier. An explanation for the metal dependence can be provided as well: the shorter the M–P distances (Os–P > Ru–P > Fe–P), the higher the congestion in the coordination sphere that would hinder the hydride motion. *Electronic* contributions can also be very important, although it is difficult to evaluate qualitatively relative energies of the structures in Scheme 3 with different PR_3 and M centers.

The idea, that intramolecular hydride traversing of the L–M–L edges is responsible for the fluxional NMR behavior of many MH_nL_m complexes, originates from the early 1970s.[1] Interesting for the present study is that the first complexes analyzed in terms of the tetrahedral jump model were dihydrides of iron and ruthenium, $M(H)_2(PR_3)_4$, closely related to the neutral precursors of the cationic complexes of this work.

An essential structural feature of the dihydrides is that they are quite distorted octahedrons. Their $[MP_4]$ skeletons tend to adopt pseudotetrahedral arrangement around the metal, although some of the P–M–P angles remain relatively small (98–99° in $Fe(H)_2(PhP(OEt)_2)_4$), while the *trans* P–M–P angle is quite large (136.7° in this example).[36]

Given that the same mechanism, tetrahedral jump, is operative in both the dihydrides and the cationic trihydride molecules of the T structure, these two systems demonstrate distinctly different dynamic behavior. Contrary to the $[M(H)_3(PR_3)_4]^+$ system, the dihydrides are *more fluxional* with *lighter* M and *bulkier* PR_3. For example, $Fe(H)_2(PEt_3)_4$ shows a broad exchanging ^{31}P A_2B_2 pattern at 20 °C, while well-resolved resonances are observed at this temperature for $Fe(H)_2(PMe_3)_4$ and $Ru(H)_2(PEt_3)_4$.

It has been suggested[1c] that in $M(H)_2(PR_3)_4$ (a) "...the contribution of the phosphorus skeletal rearrangement to the barrier should decrease with bulkier ligands..." and (b) "...the increase in barrier on going from iron to ruthenium as central atom is consistent with decreased steric push toward a regular tetrahedron due to increased metal covalent radius".

It might be as well that the nature of the trend is mostly *electronic* instead. By analogy with the transformations shown in Scheme 3, the transition geometry of $M(H)_2(PR_3)_4$ can be a distorted octahedron with *trans*-hydrides. The relative stability of the *cis*- and *trans*-dihydride isomers with different metals would then determine the fluxional properties. Theoretical calculations might evaluate the periodic trends and provide better understanding for the relative contribution of the steric and electronic factors.[37]

c. Isomerization between C_n and T Isomers. The third and rather slow dynamic process observed in this work is the $[C \rightleftharpoons T]$ isomerization of $[FeH_3(PMe_3)_4]^+$, $[RuH_3(PEt_3)_4]^+$, and $[OsH_3(PMe_3)_4]^+$. In none of these cases was it feasible to isolate and provide detailed (X-ray) structural characterization for both types of isomers. The two solid-state structures of $[FeH(H_2)(PMe_3)_4]^+$ and $[Fe(H)_3(PEt_3)_4]^+$ can be recalled here to envisage an isomerization mechanism that takes place on the NMR time scale in **1a**.

Structure **1a**,C_n (Figure 12) shows a specific view of this molecule with the three phosphines numbered P_2, P_3, and P_4 confined to the plane of the figure. An analogous representation can be achieved (not shown) viewing from the P_4 side and confining P_1, P_2, and P_3 to one plane. The second experimental geometry of **1b**,T is meant to be a structural model for **1a**,T.

(36) Guggenberger, L. J. *Inorg. Chem.* **1973**, *12*, 1317.
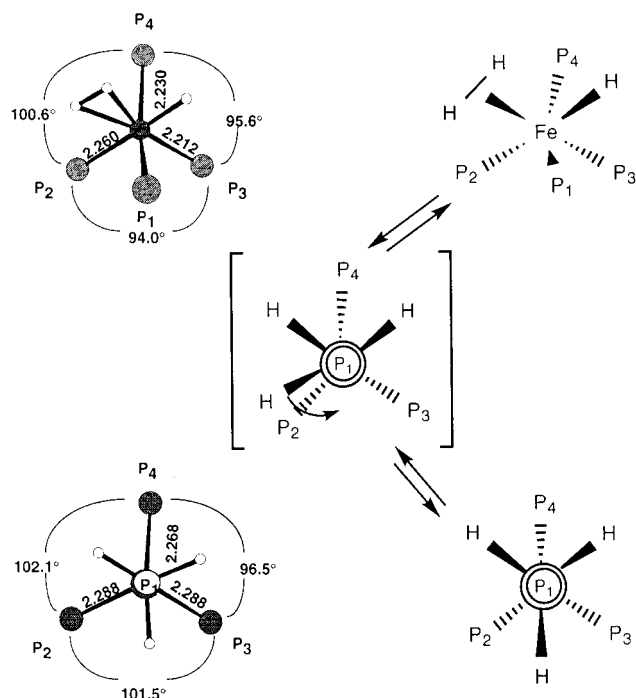(37) Berke, H.; Jacobsen H. *Chem. Eur. J.* **1997**, in press.

Figure 12. Proposed mechanism of the isomerization of [FeH₃-(PMe₃)₄]⁺ in solution, reconstructed using the solid-state structures of **1a**,C_n and **1b**,T. Characteristic distances and angles are given in the figure.

Many features of the skeleton of these structures **1a**,C_n and **1b**,T are quite similar and therefore excessive heavy ligand motion is not required during the isomerization process.

A transition structure suggested in the center of Figure 12 emphasizes two essential coordinates for the [$C \rightleftharpoons T$] rearrangement: bending of the Fe—P₁ bond and hydrogen jump over the P1—P2 edge. The P₁—Fe—P₂ (102.1°) angle in **1a**,C_n compares well to the P—Fe—P angles in the T structure and therefore the rise in energy associated with the edge crossing might be comparable in both molecules. On going from C_n to T the hydrogen motion is accompanied by the Fe—P₁ bending. An alternative for this is a jump over the P₂—P₄ edge, i.e., motion that would require bending of the Fe—P₄ vector. What is difficult to show in the transition state structure of Figure 12 is that the P₂ and P₃ ligands should slightly drift toward the departing phosphine (P₁ in Figure 12) to complete the isomerization.

A barrier for the **1a**,T to **1a**,C_n isomerization can be estimated from the exchange-broadened ¹H{³¹P} NMR spectra simulated with the DNMR5 program. An activation energy $\Delta G^{\ddagger}$ of 8.8(2) kcal/mol is found in the temperature range from −70 to −90 °C, where the two resonances coalesce in the hydride region. The isomerization of **3a**,T to **3a**,C_n has a comparable barrier of 9.1(2) kcal/mol at −80 °C (the decoalescence in this system is observed between −60 and −70 °C). Both are slightly higher than the barriers for the tetrahedral jumps of the **1a**,T and **3a**,T structures estimated as 7.8(1) kcal/mol (−100 to −120 °C, Fe) and <6.4 kcal/mol (Os).

VI. Acidity of the [MH₃(PR₃)₄]⁺ Complexes (1−3)

Weak Brønsted acidity is an intrinsic chemical property of the cationic hydrides [MH₃(PR₃)₄]⁺. In this section, we attempt the determination of the pK_a values for complexes **1−3** by NMR spectroscopy.

(38) (a) Kristjansdottir, S. S.; Norton, J. R. *In Transition Metal Hydrides: Recent Advances in Theory and Experiment*; Dedieu, A., Ed.; VCH, New York, 1991; Chapter 10.

An approximate pK_a (pseudoaqueous value) can be obtained by NMR determination of the equilibrium constant K_{eq} for the reaction between a suitable acid (BH⁺) of known pK_a and the conjugate hydride precursor (MH$_n$L$_m$) of the protonated complex [MH$_{n+1}$L$_m$]⁺:[3c,38]

$$MH_nL_m + BH^+ \rightleftharpoons [MH_{n+1}L_m]^+ + B$$
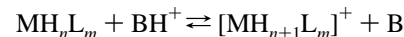
$$pK_a([MH_{n+1}L_m]^+) = pK_a(BH^+) + \log(K_{eq})$$

Thermodynamic acidities have been reported for complexes of the *trans*-[MH(H₂)(P−P)₂]⁺ (P−P = bidentate phosphine)[3] and [Ru(C₅R₅)(H₂)(PR₃)]⁺ families.[28] The pK_a values range from 4 to 16 for these molecules with increasing basicity of the phosphine resulting in decreasing acidity of the [MH$_{n+1}$L$_m$]⁺.

All pseudoaqueous pK_a([MH$_{n+1}$L$_m$]⁺) values available in the literature have been referenced to the phosphonium salts, BH⁺ = HPR₃⁺, of different acidity.[3c,38] This approach is certainly based on two assumptions (which, however, have never been addressed experimentally) that (a) the difference pK_a(BH⁺) − pK_a([MH$_{n+1}$L$_m$]⁺) should be the same in THF and water and (b) the difference pK_a(HPR′₃⁺) − pK_a(HPR″₃⁺) in THF is unchanged when compared to that in water.

The complexes [MH₃(PR₃)₄]⁺ are not amenable to any acidity determination by NMR in H₂O because of the low water solubility of the neutral dihydrides. All M(H)₂(PMe₃)₄ are well-soluble in methanol, which among the organic solvents has acid/base properties closest to water. The acidity of a number of hydride complexes (HB) has already been determined by measuring the rates k_1 and k_{-1} of the reaction:

$$HB + CH_3O^- \rightleftharpoons B^- + CH_3OH$$
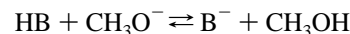
The pK_a values have been calculated from the difference pK_s − $\log(k_1/k_{-1})$, where K_s is the ion product of methanol, pK_s = 16.7.[39]
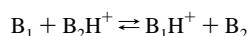
The strategy employed in these experiments involved (a) determination of the equilibrium constant K_{eq} for the protonation of M(H)₂(PMe₃)₄ by methanol (in methanol), (b) calculation of pK_a([MH₃(PMe₃)₄]⁺) = pK_a(CH₃OH) + $\log(K_{eq})$, and (c) determination of the acid/base equilibria between [OsH₃-(PMe₃)₄]⁺ and M(H)₂(PR₃)₄ in THF-d_8. The results of these experiments are collected in Table 3.

The complexes M(H)₂(PMe₃)₄ are reversibly protonated by methanol (pK_a(CH₃OH) = 15.5), and the equilibrium favors the *dihydrides*. The equilibrium constants given in Table 3 (nos. 3, 8, and 9) estimate very similar pK_a of [RuH(H₂)(PMe₃)₄]⁺ and [Os(H)₃(PMe₃)₄]⁺ as 11.3 and 11.5 (the error is at least ± 0.1). The second value is an apparent acidity, pK_a(**3a**), of the complex which actually exists in two isomeric forms in solution. The apparent pK_a must be greater that the actual pK_a of the isomers.[38] For the present case, pK_a(**3a**,C_c) = pK_a(**3a**) − log-(1+1/K_1) and pK_a(**3a**,T) = pK_a(**3a**,C_c) − $\log(K_1)$, K_1 = [**3a**,C_c]/[**3a**,T].

With the equilibrium constant K_1 = ca. 7 (see discussion in section IIIb), the values pK_a(**3a**,C_c) = ca. 11.4 and pK_a(**3a**,T) = ca. 10.6 result. The pK_a of the more abundant isomer is always close to the apparent pK_a; the difference is maximal (0.3 pK units) when K_1 = 1.[38] The value for the less abundant isomer can be determined less reliably.

A cross-experiment of protonation of Ru(H)₂(PMe₃)₄ by [Os-(H)₃(PMe₃)₄]⁺ in THF-d_8 (Table 3, no. 2) established an

(39) (a) Walker, H. W.; Kresge, C. T.; Ford, P. C.; Person, R. G. *J. Am. Chem. Soc.* **1979**, *101*, 7428. (b) Walker, H. W.; Pearson, R. G.; Ford, P. C.; *J. Am. Chem. Soc.* **1983**, *105*, 1179. (c) Pearson, R. G. *Chem. Rev.* **1985**, *85*, 41.

Table 3. Acid/Base Equilibria for the Complexes $[MH_3(PR_3)_4]^+/MH_2(PR_3)_4$ at 20 °C

$$B_1 + B_2H^+ \rightleftharpoons B_1H^+ + B_2$$

N	$[B_1]$, mol/L	$[B_2H]^+$, mol/L	solvent	K_{eq}, (¹H)/(³¹P)[a]	ΔpK_a[b], (¹H)/(³¹P)[a]	pK_a[c], $[MH_3(PMe_3)_4]^+$
1	$FeH_2(PMe_3)_4$, 0.064	$[OsH_3(PMe_3)_4]^+$, 0.028	THF-d_8	0.117/0.120	−0.93/−0.92	10.6, $[FeH_3(PMe_3)_4]^+$
2	$RuH_2(PMe_3)_4$,, 028	$[OsH_3(PMe_3)_4]^+$, 0.024	THF-d_8	0.478/−[d]	−0.32/−[d]	11.2, $[RuH_3(PMe_3)_4]^+$
3	$RuH_2(PMe_3)_4$, 0.049	CH_3OH, 24.686	CH_3OH	−/0.000060	−/−4.2	11.3, $[RuH_3(PMe_3)_4]^+$
4	$RuH_2(PEt_3)_4$, 0.017	$[OsH_3(PEt_3)_4]^+$, 0.025	THF-d_8	−[e]/0.0058	−[e]/−2.2	11.0, $[RuH_3(PEt_3)_4]^+$
5	$OsH_2(PMe_3)_4$, 0.037	$[RuH_3(PEt_3)_4]^+$, 0.033	THF-d_8	3.14/3.25	0.50/0.51	11.0, $[RuH_3(PEt_3)_4]^+$
6	$RuH_2(PEt_3)_4$, 0.026	$HPCy_3^+$, 0.031	THF-d_8	−/>600	−/>2.8	>12.5,[f] $[RuH_3(PEt_3)_4]^+$
7	$RuH_2(PEt_3)_4$, 0.027	$HP^tBu_3^+$, 0.031	THF-d_8	−/>700	−/>2.8	>14.2,[g] $[RuH_3(PEt_3)_4]^+$
8	$OsH_2(PMe_3)_4$, 0.043	CH_3OH, 24.686	CH_3OH	−/0.000124	−/−3.91	11.6, $[OsH_3(PMe_3)_4]^+$
9	$OsH_2(PMe_3)_4$, 0.054	CH_3OH, 24.686	CH_3OH	−/0.000085	−/−4.07	11.4, $[OsH_3(PMe_3)_4]^+$
10	$OsH_2(PEt_3)_4$, 0.033	$[OsH_3(PMe_3)_4]^+$, 0.037	THF-d_8	56.2/50.2	1.75/1.70	13.2, $[OsH_3(PEt_3)_4]^+$
11	$OsH_2(PEt_3)_4$, 0.018	C_2H_5OH, 17.387	C_2H_5OH	−/0.000073	−/−4.14	11.8, $[OsH_3(PEt_3)_4]^+$
12	$OsH_2(PEt_3)_4$, 0.033	C_2H_5OH, 17.387	C_2H_5OH	−/0.000082	−/−4.09	11.8, $[OsH_3(PEt_3)_4]^+$
13	PCy_3, 0.071	$HP^tBu_3^+$, 0.034	THF-d_8	−/0.14	−/−0.85[h]	11.4[40]
14	P^nBu_3, 0.071	$HPCy_3^+$, 0.034	THF-d_8	−/0.15	−/−0.82[i]	9.7[41]

[a] ¹H and ³¹P NMR data, respectively. [b] Determined as $\log(K_{eq}) = pK_a(B_1H^+) - pK_a(B_2H^+)$. [c] Referenced to the pK_a of $[Os(H)_3(PMe_3)_4]^+$ determined in methanol as 11.5, see Discussion. [d] The ³¹P NMR resonance of $[RuH_3(PMe_3)_4]^+$ is broad at 20 °C, this makes accurate integration difficult. [e] Not determined, because of the overlapping RuH_2 and OsH_3 chemical shifts. [f] Referenced to $pK_a(HPCy_3^+) = 9.7$. [g] Referenced to $pK_a(HP^tBu_3^+) = 11.4$. [h] The difference ΔpK_a (pseudoaqueous scale) was determined by titration in CH_3NO_2 as 1.75.[40] [i] The difference ΔpK_a (pseudoaqueous scale) was determined by titration in CH_3NO_2 as 1.27.[41]

equilibrium with $\log(K_{eq}) = \Delta pK_a = -0.3$, in agreement with the result of the two independent determinations in methanol. The differences in solvation energies of the bulky $M(H)_2(PR_3)_4$ and $[MH_3(PR_3)_4]^+$ cations appear similar in methanol and THF, and thus, the *relative* acidity of complexes **1**−**3** can be measured in THF on the pseudowater scale.

The pK_a of $[Os(H)_3(PMe_3)_4]^+$ (11.5) was chosen as an internal reference in this work mostly because of its high stability. This trihydride does not dissociate PMe_3 during the time (0.5 to 3 h), which is necessary for the establishment of the acid/base equilibria. Within this time, the other examples, complexes **1** and **2**, show PMe_3/PEt_3 scrambling when mixed, which prevents any reliable measurements.

The pK_a values of $[MH_3(PR_3)_4]^+$ show the following order: **3b** (13.2) > **3a** (11.5) > **2a** (11.2) > **2b** (11.0) > **1a** (10.6). The pK_a determination was impossible with **1b**, because of a fast reaction between $[Fe(H)_3(PEt_3)_4]^+$ and its conjugated base $Fe(H)_2(PEt_3)_4$ that produced stable $Fe(H)_2(H_2)(PEt_3)_3$. The apparent value of $pK_a(\mathbf{2b})$ should be taken as acidity of the classical trihydride **2b**,*T*. This is very close to the pK_a of the dihydrogen complex $[RuH(H_2)(PMe_3)_4]^+$ (**2a**,*C_n*). The less abundant dihydrogen isomer **2b**,*C_n* must be more acidic. This is opposite to **1a** where the dihydrogen complex **1a**,*C_n* (pK_a = ca. 10.5) is more basic, since the trihydride isomer **1a**,*T* is thermodynamically less stable.

Only the most basic of the dihydrides, $Os(H)_2(PEt_3)_4$, was detectably protonated by ethanol, which is less acidic than methanol (($pK_a(C_2H_5OH) = 15.9$). Two determinations (Table 3, nos. 11 and 12) both have found a higher acidity of $[Os(H)_3(PEt_3)_4]^+$ in C_2H_5OH than in CH_3OH, pK_a = 11.8 *vs* 13.2, respectively. These and the others pK_a values in Table 3 are only pseudoaqueous values and to a certain extent are influenced by the solute/solvent interactions in the solvent of determination. All PEt_3 derivatives of $M(H)_2L_4$ are notably less soluble than those of PMe_3 in alcohols, especially in methanol. The thermodynamic acidity might be increased if the protonated $[Os(H)_3(PEt_3)_4]^+$ is then even less soluble, i.e., thermodynamically destabilized by the interaction with the solvent. In this respect, the pK_a values permit a reliable comparison of *relative* acidity, if measured in one and the same solvent (e.g., THF in this series) in which compounds to be compared are all well-soluble.

Except for $[Os(H)_3(PEt_3)_4]^+$, all complexes of this work are markedly *more acidic* than the corresponding *trans*-$[MH(H_2)$-

$(P-P)_2]^+$ (P−P = dmpe, depe). Qualitatively this is established by the different behavior in methanol: $Ru(H)_2(PMe_3)_4$ and $Os(H)_2(PMe_3)_4$ are protonated to give less than 25% of the cations in solution. On the contrary, all $M(H)_2(P-P)_2$ are completely protonated by CH_3OH and establish equilibria in C_2H_5OH which strongly favor the protonation product.[3,11] The equilibrium concentrations have been reported for $Fe(H)_2(dmpe)_2/[FeH(H_2)$-$(dmpe)_2]^+$ (1:5 at −6 °C, total concentration of 67 mM)[3a] and $Ru(H)_2(dmpe)_2/[RuH(H_2)(dmpe)_2]^+$ (3:5 at 12 °C, total concentration of 41 mM).[3d] These lead to estimated pK_a values of 14.1 (Fe) and 13.3 (Ru) in ethanol at the respective temperatures, determined as $15.9 + \log(K_{eq})$ with the equilibrium constants $K_{eq} = $ [dihydrogen complex][EtO⁻]/([dihydride][EtOH]).

In addition to this, the temperature dependence of K_{eq} was determined, which led to $\Delta H = -8.8$ kcal/mol and $\Delta S = -45.9$ eu for $Fe(H)_2(dmpe)_2/[FeH(H_2)(dmpe)_2]^+$ and to $\Delta H = -6.0$ kcal/mol and $\Delta S = -19.9$ eu for $Ru(H)_2(dmpe)_2/[RuH(H_2)$-$(dmpe)_2]^+$.[3a,d] In both cases the equilibrium constants at 20 °C should be smaller than those reported at −6 and 12 °C. There is some ambiguity in the original publications concerning the definition of this equilibrium constant. It appeared as if it was measured as the ratio $M(H)_2(dmpe)_2/[MH(H_2)(dmpe)_2]^+$ in both cases. This predicts the $Ru(H)_2(dmpe)_2/[RuH(H_2)(dmpe)_2]^+$ ratio of 3:4 at 20 °C and pK_a = 13.2. We cannot however securely interpret the thermodynamic parameters for $Fe(H)_2$-$(dmpe)_2/[FeH(H_2)(dmpe)_2]^+$, since there is no apparent way to reproduce the ratio (1:5) reported at −6 °C. In a recent review,[38] the pK_a of $[FeH(H_2)(dmpe)_2]^+$ was estimated from the mentioned equilibrium data as ∼12. It results from the sum $15.9 + \log(K_{eq})$ with the K_{eq} value formally calculated from the ΔH and ΔS at 293 K.

The observation of higher acidity of $[MH_3(PR_3)_4]^+$ *vs* $[MH$-$(H_2)(P-P)_2]^+$ (R = Me, Et, and P−P = dmpe, depe) is presumably determined more by the different thermodynamic stability of the conjugate bases $M(H)_2(PR_3)_4$ and $M(H)_2(P-P)_2$ rather than by any electronic difference between the ligands.[38] All $M(H)_2(PR_3)_4$ of this work are exclusively *cis*-dihydrides in solution, while the dihydrides $M(H)_2(P-P)_2$ form equilibrium mixtures of the *cis*- and *trans*-isomers when dissolved,[3a,d,11] which indicates that the lower energy *cis*-structure can be destabilized by the chelating phosphorus ligands.

The pK_a difference between $[MH_3(PR_3)_4]^+$ and the standards of previous determinations, $HPCy_3^+$ and $HP^tBu_3^+$, cannot be

M(II) and M(IV) Complexes [MH₃(PR₃)₄]⁺

J. Am. Chem. Soc., Vol. 119, No. 16, 1997 3729

established experimentally. Even one of the least basic complexes Ru(H)$_2$(PEt$_3$)$_4$ is completely protonated by both of these acids in THF-d_8 (Table 3, nos. 6 and 7). The equilibrium constants in this case must be more than $600-700$ based on the experimental [PR$_3$]/[HPR$_3^+$] ratios (ca. $6-7$, see concentrations in Table 3) and the assumption that the ratio [RuH$_3$-(PEt$_3$)$_4^+$]/[RuH$_2$(PEt$_3$)$_4$] must be more than 100, if for the second species the ^{1}H and ^{31}P NMR detection limit is reached. The pK_a of [RuH$_3$(PEt$_3$)$_4$]$^+$ then must be greater than pK_a(HP^{t}Bu$_3^+$) + log(K_{eq}) = 11.4[40] + 2.8, i.e., >14.2. Consequently, the pK_a of our standard complex **3a** should be greater than 14.7 on a scale referenced to HP^{t}Bu$_3^+$ (*vs* 11.5 determined here in methanol). This we are reluctant to accept, since at this acidity the protonation of all our complexes **1**−**3** should have been practically complete in both CH$_3$OH and C$_2$H$_5$OH. We also found no detectable formation of HP^{t}Bu$_3^+$ in a 0.12 M solution of P^{t}Bu$_3$ in CH$_3$OH, indicating that the pK_a of HP^{t}Bu$_3^+$ is less than 11.4 in this alcohol.

Table 3 also shows results of two additional experiments: protonation of PCy$_3$ by HP^{t}Bu$_3^+$ and protonation of P^{n}Bu$_3$ by HPCy$_3^+$ (nos. 13 and 14) in THF-d_8. The measured difference ΔpK_a is 0.85(5) between HP^{t}Bu$_3^+$ and HPCy$_3^+$ and 0.82(5) between HPCy$_3^+$ and HP^{n}Bu$_3^+$. These differences (pseudoaqueous scale) are known as 1.75[40] and 1.27,[41] respectively, from the potentiometric titration experiments in CH$_3$NO$_2$. Thus, it appears, that even the phosphines of a close basicity range show a significantly contracted pK_a scale in THF (total 1.67 pK_a units in THF *vs* 3.02 in the literature data). Any determination referenced with HPR$_3^+$ spanning a larger range can therefore be endangered by significant errors both in the absolute (on the pseudoaqueous scale) and relative acidity of [MH$_{n+1}$L$_m$]$^+$.

More work is necessary to verify if ΔpK_a([MH$_{n+1}$L$_m$]$^+$ − HPR$_3^+$) is comparable in different solvents like THF and H$_2$O. This would require preparation of a series of complexes with at least one representative of known pK_a in H$_2$O (or CH$_3$OH) and one which is reversibly protonated by HP^{t}Bu$_3^+$, with the *mutual* acid/base properties also established in THF.

VII. Experimental Section

When not mentioned otherwise, all operations were performed under an atmosphere of N$_2$ using standard Schlenk and glovebox techniques. All solvents were rigorously dried over an appropriate drying agent, followed by distillation under N$_2$. Deuterated solvents used in the NMR experiments were dried over sodium (C$_6$D$_6$, THF-d_8) or P$_2$O$_5$ (CD$_2$-Cl$_2$) and vacuum transferred for storage in Schlenk flasks fitted with Teflon stopcocks. The CDFCl$_2$/CDF$_2$Cl mixture was prepared by a reported procedure.[42] Anhydrous CH$_3$OH (Aldrich) was vacuum-distilled before use in the acidity measurements.

For the NMR experiments typically a solid [MH$_3$(PR$_3$)$_4$]$^+$ sample was weighed in a 5-mm NMR tube in the glovebox. The charged tube was tightly fitted into a small apparatus closed with Teflon stopcock that preserved the inner space from passage of air during subsequent manipulations. This apparatus was removed from the box, attached to a vacuum line, and evacuated, and then the solvent was vacuum-transferred into the tube. The tube could be flame-sealed under 850 Torr of Ar, H$_2$, or under vacuum. This provided solutions of [MH$_3$-(PR$_3$)$_4$]$^+$ prepared between −80 and −100 °C. The NMR experiments were started below −90 °C. This was important for complexes **1** and **2** in CDFCl$_2$/CDF$_2$Cl which slowly decomposed in this solvent at room temperature.

All NMR experiments were carried out on a Varian Gemini 300 spectrometer. ^{1}H NMR spectra were referenced to the residual proton resonance of the deuterated solvent. ^{31}P chemical shifts were externally referenced to 85% H$_3$PO$_4$ sealed in a capillary and inserted into a standard 5-mm NMR tube filled with the deuterated solvent. ^{1}H T_1 measurements were performed at 300 MHz using the inversion recovery method. A long repetition time of 20 s was employed for the equilibrium constant determinations by ^{1}H and ^{31}P NMR (Table 3). This was typically more than $3T_1$ relaxation times of the integrated lines. In the experiments in CH$_3$OH and for the protonation of PR$_3$ by HPR$'_3$,$^+$ the acids and conjugated bases were in fast exchange on the relaxation time scale at 20 °C according to the T_1 time estimates. Therefore, the ratios [B]/[BH$^+$] and the reported K_{eq} (Table 3) are not affected by any relaxation effects.

Rate constants for the intramolecular exchange (hydride jump) in all *T* isomers were determined by simulation of the exchange-broadened ^{31}P{^{1}H} NMR spectra using the DNMR5 program.[43] The model assumed a mutual exchange (MU = 1) between four nuclear configurations of four nuclei (1234, 2134, 3214, and 4231). The isomerization [*C* ⇌ *T*] was modeled as a two-site exchange. Experimental T_1 times were used for the simulations of all ^{1}H{^{31}P} NMR spectra, while reasonable line widths ($2-3$ Hz) were employed for the ^{31}P spectra. During the simulation the rate constants were iterated to reach a close agreement between the calculated and experimental line widths and intensities.

The following reagents were from commercial suppliers: [NBu$_4$]BH$_4$, NaBH$_4$, NaBPh$_4$, (CF$_3$)$_2$CHOH (Aldrich), anhydrous FeCl$_2$ (Fluka), RuCl$_3$·nH$_2$O (assay 42.12%, Johnson Matthey Co.), OsO$_4$ (Johnson Matthey Co.). K$_2$[OsO$_2$(OMe)$_4$] was prepared by the method of Criegee.[44]

Preparation of the Dihydrides M(H)$_2$(PR$_3$)$_4$. Dihydridotetrakis-(trimethylphosphino)iron(II), Fe(H)$_2$(PMe$_3$)$_4$. PMe$_3$ (3.9 mL, 37.7 mmol) was added to a suspension of FeCl$_2$ (0.6 g, 4.7 mmol) in 30 mL of ethanol. The mixture was stirred for 1 h. To the resulting clear, almost colorless solution was added NaBH$_4$ (0.36 g, 9.5 mmol), and the dark lilac reaction mixture was left stirring for 2.5 h. The solvent was then removed completely *in vacuo*, and the residue was extracted with hexane. The solvent was removed again, and the resulting solid was sublimed (80 °C, 4×10^{-2} Torr) to afford a light yellow product: yield 0.53 g (31%). The yield of Fe(H)$_2$(PMe$_3$)$_4$ depended on the relative amount of NaBH$_4$ and PMe$_3$. In a reaction of FeCl$_2$ (0.61 g, 4.8 mmol) with 3 mL PMe$_3$ (29.9 mmol) and 0.55 g NaBH$_4$ (14.5 mmol), the sublimation afforded 1.14 g (65%) of Fe(H)$_2$(PMe$_3$)$_4$. Fe-(H)$_2$(PMe$_3$)$_4$ is extremely air-sensitive and is thermally unstable at 20 °C. When kept under N$_2$ in a drybox in a tightly closed bulb, it slowly (days) changes the color from light yellow to green. ^{1}H NMR (THF-d_8): δ 1.27 (s, PCH$_3$), −14.46 (m, FeH$_2$). ^{31}P{^{1}H} NMR (THF-d_8): an A$_2$B$_2$ pattern centered at δ 24.68, δ_A 24.32, δ_B 25.03 (^2J(A−B)) = 29.7 Hz).

The residue which remained in the first preparation after extraction with hexane as described above was additionally extracted with CH$_2$-Cl$_2$, the solvent was removed *in vacuo*, and the resulting solid was redissolved in 10 mL of methanol. Addition of 0.82 g of NaBPh$_4$ (2.4 mmol) in 5 mL of methanol to this solution precipitated violet [(PMe$_3$)$_3$-Fe(μ-H)$_3$Fe(PMe$_3$)$_3$]BPh$_4$ (reported in detail elsewhere): yield 0.67 g, 32%. ^{1}H NMR (CD$_2$Cl$_2$): δ 1.44 (m, PCH$_3$), −22.40 (sept, Fe(μ-H)$_3$-Fe, ^2J(H−P) = 8.6 Hz). ^{31}P{^{1}H} NMR (CD$_2$Cl$_2$): δ 35.1 (s). Anal. Calcd. for C$_{42}$H$_{77}$BFe$_2$P$_6$: C, 56.65; H, 8.72. Found: C, 56.53; H, 8.81.

Dihydridotetrakis(triethylphosphino)iron(II), Fe(H)$_2$(PEt$_3$)$_4$. A mixture of FeCl$_2$ (0.5 g, 3.94 mmol) and PEt$_3$ (6 mL, 40.63 mmol) was stirred for 0.2 h in 40 mL of ethanol to form a clean colorless solution. NaBH$_4$ (0.45 g, 11.90 mmol) was added, and after 24 h of stirring, a white precipitate was filtered from the orange reaction solution. The solvent was then removed *in vacuo*. The residue was extracted with 3 × 20 mL of hexane affording a solution of Fe(H)$_2$-(N$_2$)(PEt$_3$)$_4$ and a yellow solid of BH$_2$[(PEt$_2$)$_3$Fe(H)$_2$]$_2$OEt (0.43g (25%)). This complex could be dissolved in 10 mL of methanol and reprecipitated as a BPh$_4^+$ salt by the addition of NaBPh$_4$ in methanol (reported in detail elsewhere).

Fe(H)$_2$(N$_2$)(PEt$_3$)$_3$. The above hexane extract was evaporated, and the oily residue was dried under vacuum for 3 h. Addition of 15 mL of pentane caused precipitation of PEt$_3$·BH$_3$, and the mixture was left

(40) Allman, T.; Goel, R. G. *Can. J. Chem.* **1982**, *60*, 716.
(41) Streuli, C. A. *Anal. Chem.* **1960**, *32*, 985.
(42) Siegel, J. S.; Anet, F. A. L. *J. Org. Chem.* **1988**, *53*, 2629.
(43) Available from the QCPE at Indiana University (QCMP 059)
(44) Criegee, R. *Ann.* **1942**, *550*, 99.

overnight at -30 °C. The cold mother liquor was quickly removed from the precipitate via a cannula and dried under vacuum to give about 1.2 g of oily $Fe(H)_2(N_2)(PEt_3)_3$: yield, ca. 70%. This oil showed at least 95% of $Fe(H)_2(N_2)(PEt_3)_3$ in the ^1H and ^{31}P NMR. It also contained about 4% of $Fe(H)_2(H_2)(PEt_3)_4$ and less than 1% of remaining $PEt_3 \cdot BH_3$.

The preparation of $Fe(H)_2(PEt_3)_4$ was continued by dissolving 0.8 g of $Fe(H)_2(N_2)(PEt_3)_3$ in 5 mL of PEt_3 in a Schlenk flask fitted with Teflon closure. The flask was heated to 45 °C under vacuum, stirred for 2 days, and repeatedly degassed from evolving N_2. The formed $Fe(H)_2(PEt_3)_4$ was kept in the PEt_3 solution under Ar to prevent thermal decomposition. A typical isolation of solid $Fe(H)_2(PEt_3)_4$ included the following: PEt_3 was removed from ca. 0.7 mL of the $Fe(H)_2(PEt_3)_4$ solution in PEt_3, and the yellow solid was dried under vacuum, cooled to -70 °C, and washed under Ar with 3×2 mL of cold (-70 °C) methanol, which could be conveniently removed from the solid with a pipet. The afforded light yellow $Fe(H)_2(PEt_3)_4$ was dried under vacuum: yield, 80−90 mg, 60−67%. This solid complex can be handled under N_2 for a short time (1 h) at room temperature without apparent decomposition. Data for $BH_2[(PEt_3)_3Fe(H)_2]_2BPh_4$. ^1H NMR (CD_2Cl_2): δ 1.68 (m, PCH_2), 1.15 (m, PCH_2CH_3), -14.24 (br. m, FeH_3). $^{31}P\{^1H\}$ NMR (CD_2Cl_2): δ 49.1 (s). $^{11}B\{^1H\}$ NMR (CD_2Cl_2): δ 0.0 (s, BPh$_4^-$), 66.2 (br. s, $\Delta = 370$ Hz, Fe$-B-$Fe). Anal. Calcd. for $C_{60}H_{116}B_2Fe_2P_6$: C, 62.30; H, 10.11. Found: C, 62.45; H, 9.92. Data for $Fe(H)_2(N_2)(PEt_3)_3$. ^1H NMR (C_6D_6): δ 1.56 (br. m, PCH_2), 1.08 (m, PCH_2CH_3), -17.21 (ddt, FeH, ^2J(H−H) $= 17.6$ Hz, ^2J(H−P) $= 50.1$, 61.9 Hz), -12.89 (ddt, FeH, ^2J(H−P) $= 28.2$, 76.6 Hz). $^{31}P\{^1H\}$ NMR (C_6D_6): δ 56.5 (d, ^2J(P−P) $= 18.1$ Hz), 49.7 (t). Data for $Fe(H)_2(H_2)(PEt_3)_3$. ^1H NMR (C_6D_6) δ -12.20 (q, FeH_4, ^2J(H−P) $= 28.4$ Hz). ^{31}P NMR (C_6D_6): δ 65.5 (s), quintet in the hydride-coupled spectrum. Data for $Fe(H)_2(PEt_3)_4$. ^1H NMR (C_6D_6, 21 °C): δ 1.59 (m, PCH_2), 1.06 (m, PCH_2CH_3), -15.94 (multiplet with three broad inner and two sharp outer lines, FeH_2, the separation between the outer sharp lines is 183.9 Hz). ^{31}P NMR (C_6D_6, 21 °C): δ 46.5 (br. s, $\Delta = 133$ Hz), 51.3 (br. s, $\Delta = 131$ Hz).

Dihydridotetrakis(trimethylphosphino)ruthenium(II), $Ru(H)_2(PMe_3)_4$. PMe_3 (2 mL, 19.3 mmol) was dissolved in 15 mL of THF and added into a very dark mixture of $RuCl_3 \cdot nH_2O$ (0.377, 1.57 mmol) in 15 mL of THF. This immediately afforded a brown precipitate. After 1 h of stirring, $[NBu_4]BH_4$ (1.22 g, 4.74 mmol) was added, and the stirring was continued for an additional 2 h to give a dark yellow solution with some precipitate of $[NBu_4]Cl$. This was filtered, and the THF was removed completely. The residue was extracted with 5×30 mL of pentane. The solvent was then removed again to give a solid, which was dried *in vacuo* for 6 h to afford spectroscopically pure $Ru(H)_2(PMe_3)_4$: yield, 0.45 g, 70%. The purity of this material was sufficient for the subsequent preparation of **2a**. The complex could be additionally purified by sublimation.[31] ^1H NMR (THF-d_8): δ -10.12 (m, RuH_2). ^{31}P NMR (THF-d_8): δ -6.9 (t, ^2J(P−P) $= 26.4$ Hz), 0.7 (t).

Dihydridotetrakis(triethylphosphino)ruthenium(II), $Ru(H)_2(PEt_3)_4$. This dihydride was prepared by the above method using 0.30 g (1.04 mmol) of $RuCl_3 \cdot nH_2O$, 1.5 mL (10.2 mmol) of PEt_3, and 1 g (3.9 mmol) of $[NBu_4]BH_4$ in 40 mL of THF. The pentane extract was, however, treated differently. The volume of the pentane solution was reduced to about 20 mL (when precipitation of $PEt_3 \cdot BH_3$ started) and left at -30 °C overnight. The cold mother liquor was quickly removed from the solid via a cannula, and the solvent was then evaporated. The residue was washed with 3×5 mL of cold (-70 °C) methanol and dried for 1 h *in vacuo* to afford spectroscopically pure $Ru(H)_2(PEt_3)_4$: yield, 0.55 g, 76%. ^1H NMR (THF-d_8): δ -11.79 (m, RuH_2). ^{31}P NMR (THF-d_8): δ 21.7 (t, ^2J(P−P) $= 20.7$ Hz), 32.1 (t).

Dihydridotetrakis(trimethylphosphino)osmium(II), $Os(H)_2(PMe_3)_4$. A mixture of $K_2[OsO_2(OMe)_4]$ (0.187 g, 0.44 mmol) and PMe_3 (0.4 mL, 3.86 mmol) was stirred in 8 mL of ethanol for about 5 min until a clear solution was formed. $NaBH_4$ (66 mg, 1.75 mmol) was added, and the stirring was continued for 1.5 h at 70 °C. After removal of the solvent *in vacuo*, the dihydride $Os(H)_2(PMe_3)_4$ was extracted with hexane to afford a crude product of approximately 90% purity according to the ^1H and ^{31}P NMR data (a detectable impurity was $OsH_4(PMe_3)_3$, ca. 4%): yield, 0.16 g, 73%. Subsequent protonation of this material by a $CH_3OH/(CF_3)_2CHOH$ mixture (see below) afforded 177 mg of

$[Os(H)_3(PMe_3)_4]BPh_4$. Pure $Os(H)_2(PMe_3)_4$ could only be recovered from this salt as described below for $Os(H)_2(PEt_3)_4$.

From the residue of the extraction, a small amount of $[OsH(PMe_3)_5]OEt$ was extracted with CH_2Cl_2, redissolved in methanol and precipitated as a BPh_4^- salt by addition of $NaBPh_4$ in methanol. Data for $[Os(CH_3)(PMe_3)_5]^+$. ^1H NMR (CD_2Cl_2): δ -0.28 (doublet of quintets, OsCH_3, ^3J(H−P) $= 3.5$, 10.9 Hz). $^{31}P\{^1H\}$ NMR (CD_2Cl_2): δ -54.9 (d, ^2J(P−P) $= 14.2$, becomes a doublet of quartets in the selectively PMe_3-decoupled ^{31}P spectrum), -64.3 (qi). Data for $[OsH(PMe_3)_5]^+$. ^1H NMR (CD_2Cl_2): δ -12.27 (doublet of quintets, OsH, ^2J(H−P) $= 54.6$, 21.9 Hz). $^{31}P\{^1H\}$ NMR (CD_2Cl_2): δ -55.7 (d, ^2J(P−P) $= 18.0$, becomes a doublet of doublets in the selectively PMe_3-decoupled ^{31}P spectrum), -60.7 (qi). Data for $Os(H)_2(PMe_3)_4$. ^1H NMR (THF-d_8): δ -11.26 (m, OsH_2). $^{31}P\{^1H\}$ NMR (THF-d_8): δ -52.8 (t, ^2J(P−P) $= 18.0$ Hz), -47.2 (t). Data for $OsH_4(PMe_3)_3$. ^1H NMR (THF-d_8): δ -10.10 (q, OsH_4, ^2J(H−P) $= 10.5$ Hz). $^{31}P\{^1H\}$ NMR (THF-d_8): δ -48.8 (s).

Dihydridotetrakis(triethylphosphino)osmium(II), $Os(H)_2(PEt_3)_4$. A mixture of $[Os(H)_3(PEt_3)_4]BPh_4$ (0.147 g, 0.15 mmol) and KOH (0.05 g, 0.89 mmol) in 5 mL of THF was stirred for 2 h. This resulted in clean formation of $Os(H)_2(PEt_3)_4$ (^{31}P NMR observation). The solution was filtered and evaporated. The residue was dried for 2 h under vacuum at 75 °C to give white crystalline $Os(H)_2(PEt_3)_4 \cdot^1/_2THF$: 0.094 g, 95%. ^1H NMR (THF-d_8): δ -13.08 (m, OsH_2). $^{31}P\{^1H\}$ NMR (THF-d_8): δ -18.8 (t, ^2J(P−P) $= 13.4$ Hz), -11.7 (t). Anal. Calcd. for $C_{24}H_{62}P_4Os \cdot 0.5THF$: C, 44.55; H, 9.49. Found: C, 44.60; H, 9.53.

Preparation of the Cationic Complexes $[MH_3(PR_3)_4]BPh_4$, 1−3. $[FeH_3(PMe_3)_4]BPh_4$ (1a), $[RuH(H_2)(PMe_3)_4]BPh_4$ (2a), $[RuH_3(PEt_3)_4]BPh_4$ (2b), $[Os(H)_3(PMe_3)_4]BPh_4$ (3a). A typical preparation of these complexes consisted of the following: 0.05 g of the corresponding dihydride was dissolved in 3 mL of $CH_3OH/(CF_3)_2CHOH$ (2:1) and mixed with a solution of 0.05 g of $NaBPh_4$ in CH_3OH to afford a precipitate of $[MH_3(PMe_3)_4]BPh_4$ which was filtered and washed with 3×2 mL of methanol and 3×2 mL of hexane or ether: typical yield, ca. 80%. In a similar manner, the preparation of the deuterium-substituted complexes **1a−3a** was achieved in CH_3OD without $(CF_3)_2$-CHOH in a lower yield of about 50%. In the preparation of **1a**, it is recommended to carry out all manipulations under argon. Otherwise it will be contaminated with $[FeH(N_2)(PMe_3)_4]BPh_4$. Anal. Calcd. for $C_{36}H_{59}BFeP_4$ (**1a**): C, 63.36; H, 8.71. Found: C, 63.67; H, 8.53. Anal. Calcd. for $C_{48}H_{83}BP_4Ru$ (**2b**): C, 64.34; H, 9.34. Found: C, 64.10; H, 9.29.

$[Fe(H)_3(PEt_3)_4][B(C_6H_3(CF_3)_2)_4]$, (1b). This preparation was carried out under an atmosphere of argon using argon-saturated solvents. A mixture of $Fe(H)_2(PEt_3)_4$ (0.062 g, 0.117 mmol) and $[Et_2O \cdot H]B(C_6H_3(CF_3)_2)_4$ (0.1 g, 0.099 mmol) was dissolved in 8 mL of ether at -70 °C. Addition of 10 mL of cold (-70 °C) hexane caused precipitation of a light yellow solid. The solid was filtered, washed with cold hexane, and dried under vacuum for 0.5 h: yield, 0.137 g, 96%. Complex **1b** is thermally unstable in solution at 20 °C. Slow decomposition (weeks) was observed in THF-d_8 in an NMR tube sealed under argon. Apparently this reaction proceeded via hydrogen loss. Compound **1b** immediately reacts in solution with $Fe(H)_2(PEt_3)_4$ to form stable $Fe(H)_2(H_2)(PEt_3)_3$, PEt_3, and some unidentified product.

Trihydridotetrakis(trimethylphosphino)osmium(IV) Tetraphenylborate, $[Os(H)_3(PEt_3)_4]BPh_4$ (3b). A mixture of $K_2[OsO_2(OMe)_4]$ (0.17 g, 0.4 mmol) and PEt_3 (0.4mL, 2.71 mmol) in 8 mL of methanol was stirred at 20 °C for 1 h. The ^{31}P NMR spectrum of the resulting clean red solution showed resonances of PEt_3 (δ -16.8), OPEt_3 (δ 60.9), $OsH_4(PEt_3)_3$ (δ 1.3), and two lines at δ -10.6 and -12.4 of $[OsH_3(PEt_3)_4]^+$ and some reactive intermediate, respectively. Formation of $[OsH_3(PEt_3)_4]^+$ was completed after 3.5 h of stirring when the solution turned almost colorless. A small amount of $OsH_4(PEt_3)_3$ (5%) was also present. This methanol reaction solution was evaporated, and the residue was extracted with 3×5 mL of hexane. The solvent was removed under vacuum, and the residue was redissolved in 10 mL of methanol. Addition of a solution of $NaBPh_4$ (0.2 g, 0.58 mmol) in 5 mL of methanol afforded a precipitate that was washed with 2×5 mL of methanol and 2×5 mL of hexane to give $[Os(H)_3(PEt_3)_4]BPh_4$: yield, 0.2 g, 51%. Anal. Calcd. for $C_{48}H_{83}BP_4Os$: C, 58.52; H, 8.49. Found: C, 58.26; H, 8.45.

M(II) and M(IV) Complexes $[MH_3(PR_3)_4]^+$

J. Am. Chem. Soc., Vol. 119, No. 16, 1997 3731

Preparation of $[HPR_3]BPh_4$ (R = Cy, ^tBu). P^tBu_3 (0.125 g, 0.62 mmol) was dissolved in 2 mL of $(CF_3)_2CHOH$, and with stirring, a slight excess of NaBPh$_4$ (0.26 g, 0.67 mmol) in 3 mL of $(CF_3)_2CHOH$/CH_3OH (2:1) was added. This immediately produced a white precipitate which was filtered, washed with 2 × 5 mL of methanol and 2 × 5 mL of hexane, and dried under vacuum to yield 0.27 g (77%) of $[HP^tBu_3]BPh_4$. $[HPCy_3]BPh_4$ was prepared with a similar yield by this above method. $^{31}P\{^1H\}$ NMR (THF-d_8): δ 63.70 (s, P^tBu_3), 57.60 (s, $HP^tBuF_3^+$), 29.95 (s, $HPCy_3^+$), 10.94 (s, PCy_3). Other ^{31}P chemical shifts from the acidity measurements in THF-d_8: −31.39 (s, P^nBu_3) and 11.87 (s, $HP^nBu_3^+$).

X-ray Structure Determination of $[FeH(H_2)(PMe_3)_4]BPh_4$ ($1a,C_n$), $[Fe(H)_3(PEt_3)_4]B(C_6H_3(CF_3)_2)_4$ ($1b,T$), and $[Os(H)_3(PMe_3)_4]BPh_4$ ($3a,C_c$). Crystals of $1a,C_n$, $1b,T$, and $3a,C_c$ were prepared by slow diffusion of hexane into solutions of ca. 10 mg of the complexes in ca. 0.4 mL of THF. The instability of $1b,T$ in solution required the preparation at −30 °C under Ar.

Intensity data were collected on a Nicolet R3 diffractometer for $1a$ and $3a$ and on a Siemens P3 diffractometer for $1b$ using graphite-monochromated Mo Kα radiation (λ = 0.710 73 Å). Crystal data, data collection, and least-squares parameters are listed in Table 4.

1a. A yellow crystal of $1a$ (0.5 × 0.45 × 0.4 mm^3) was mounted on a glass fiber with polybutene. Intensity measurements were made with 4° < 2θ < 54°. A total of 8456 reflections were collected of which 8159 were unique (R_{int} = 0.0205). The structure was solved by direct methods (SHELXTL-PLUS)[45a] and refined by full-matrix least-squares on F^2 (SHELXL−93).[45b] All atoms were refined with anisotropic displacement coefficients. The refinement converged to $R(F)$ = 0.048, wR(F^2) = 0.1114, and S = 1.102 for 7105 reflections with $F > 4σ(F_o)$ and 615 variables.

1b. A yellow crystal with approximate dimensions of 0.5 × 0.2 × 0.15 mm^3 was mounted on a glass fiber with polybutene. The orientation matrix and cell parameters were determined from 36 machine-centered reflections with 8° < 2θ < 26°. Axial photographs were used to verify the unit cell choice. A total of 14 414 reflections were collected of which 13 754 were unique (R_{int} = 0.052). The structure was solved by direct methods (SHELXTL-PLUS)[45a] and refined by full-matrix least-squares on F^2 (SHELXL−93).[45b] All non-hydrogen atoms were refined anisotropically, and hydrogen atoms were included with a model and isotropic displacement coefficients (u(H) = 0.08). The hydrogen atoms H$_1$, H$_2$, and H$_3$ were located from a difference Fourier map and refined as isotropic atoms (u(H) = 0.08). The refinement converged to $R(F)$ = 0.0729, wR(F^2) = 0.1275, and S = 1.022 for 7189 reflections with $F > 4σ(F_o)$ and 784 variables.

(45) (a) Sheldrich, G. M. SHELXTL-PLUS, Release 4.21; Siemens Analytical X-ray Instruments: Madison, Wisconsin, 1990. (b) Sheldrick, G. M. SHELXL−93. Program for the Refinement of Crystal Structures; University of Göttingen, 1993.

Table 4. Summary of Crystal Data, Details of Intensity Collection, and Least-Squares Refinement Parameters of the Complexes $1a,C_n$, $1b,T$, and $3a,C_c$.

	$1a,C_n$	$1b,T$	$3a,C_c$
chem. formula	$C_{36}H_{59}BFeP_4$	$C_{56}H_{75}BF_{24}FeP_4$	$C_{36}H_{59}BOsP_4$
fw	682.37	1394.7	816.72
a, Å	15.899(3)	12.136(2)	15.901(2)
b, Å	12.702(2)	14.205(3)	12.815(3)
c, Å	20.169(4)	37.117(6)	20.300(3)
$β$, deg	110.39(1)	98.93(1)	110.62(1)
V, Å^3	3817.9(12)	6321(2)	3871.6(12)
Z	4	4	4
space group	$P2_{1/c}$	$P2_{1/c}$	$P2_{1/c}$
T, K	153(2)	173(2)	173(2)
$λ$, Å	0.710 73	0.710 73	0.710 73
$ρ_{calcd}$, g cm^{-3}	1.187	1.466	1.401
$μ$, mm^{-1}	0.585	0.447	3.482
trans. coeff (max, min)	a	0.955, 0.9	0.997, 0.612
R, %[b]	4.80	7.29	4.88
R_w, %	11.14	12.75	11.79

[a] No absorption correction. [b] $R = \sum(||F_o| - |F_c||)/\sum|F_o|$, $R_w = \sum w^{1/2}(||F_o| - |F_c||)/\sum w^{1/2}|F_o|$.

3a. A white transparent crystal of $3a$ measuring 0.7 × 0.5 × 0.4 mm^3 was mounted on a glass fiber. Intensity measurements were made with 4° < 2θ < 54°. A total of 9105 reflections were measured of which 8797 were unique (R_{int} = 0.0463). The structure was solved by the "heavy atom" method (SHELXTL-PLUS)[45a] and refined by full-matrix least-squares on F^2 (SHELXL−93).[45b] All non-hydrogen atoms were refined with anisotropic displacement coefficients. The hydrogen atoms H$_1$, H$_2$, and H$_3$ were located from a difference Fourier map and refined as independent isotropic atoms. The refinement converged to $R(F)$ = 0.0488, wR(F^2) = 0.1179, and S = 1.038 for 6973 reflections with $F > 4σ(F_o)$ and 391 variables.

Full details are given in the Supporting Information.

Supporting Information Available: Listings of crystal data, structure determination summary, atomic coordinates, and thermal displacement parameters of the X-ray diffraction studies of **1a, 1b**, and **3a** (28 pages). See any current masthead page for ordering and Internet access instructions.